CHALMERS
UNIVERSITY OF TECHNOLOGY

Nonlinear Model Predictive Control of Active Air Suspension for Roll Stability in Tractor-Semitrailer Vehicles

Master's thesis in Mobility Engineering

Fanxiang Liao
Chaojie Lu

DEPARTMENT OF ELECTRICAL ENGINEERING
CHALMERS UNIVERSITY OF TECHNOLOGY
Gothenburg, Sweden 2026
www.chalmers.se

Master's thesis 2026

Nonlinear Model Predictive Control of Active Air Suspension for Roll Stability in Tractor-Semitrailer Vehicles

Fanxiang Liao
Chaojie Lu

CHALMERS
UNIVERSITY OF TECHNOLOGY

Department of Electrical Engineering
Chalmers University of Technology
Gothenburg, Sweden 2026

Nonlinear Model Predictive Control of Active Air Suspension for Roll Stability in Tractor-Semitrailer Vehicles
Fanxiang Liao
Chaojie Lu

Supervisor: Esteban Gelso, VOLVO TECHNOLOGY AB
Supervisor: Maliheh Sadeghi Kati, VOLVO TECHNOLOGY AB
Examiner:Jonas Fredriksson, Department of Electrical Engineering, Chalmers

Master's Thesis 2026
Department of Electrical Engineering
Chalmers University of Technology
SE-412 96 Gothenburg
Telephone +46 31 772 1000

Typeset in LaTeX
Printed by Chalmers Reproservice
Gothenburg, Sweden 2026

Nonlinear Model Predictive Control of Active Air Suspension for Roll Stability in Tractor-Semitrailer Vehicles

Fanxiang Liao
Chaojie Lu
Department of Electrical Engineering
Chalmers University of Technology

Abstract

Tractor–semitrailer combinations have a high center of gravity and strong coupling between the two vehicle units. Steering and combined steering-braking maneuvers can therefore produce large body roll and lateral load transfer. Active air suspension can reduce this risk by changing the vertical support force at each side of the tractor. Its control authority is limited by pressure, valve flow, and the pneumatic system's response speed.

This thesis builds on an earlier active air-suspension and NMPC framework. The vehicle configuration considered is a 4x2 two-axle tractor with a three-axle semitrailer. Active air suspension is installed only on the tractor, while the semitrailer keeps its passive suspension. The controller model is reformulated so that air-pressure and mass-flow dynamics are not included among the prediction states. Their physical limits are instead represented by constraints related to force, force rate, pressure, and mass flow. Pitch states and pitch weights are added. This reformulation reduces the order of the prediction model and improves computational efficiency while preserving the key actuator constraints. The model also includes forces and moments transmitted through the fifth wheel, together with a bounded preview correction for the trailer-induced roll moment.

The high-fidelity Volvo Transport Model (VTM) is used as the closed-loop simulation plant. A nonlinear two-track model provides the control-oriented vehicle prediction. The upper-layer NMPC calculates increments in tractor suspension force. A lower layer converts these force requests to pressure references and on–off valve commands.

The strategy is evaluated under step steering, ramp steering, lane change, and braking-in-a-turn maneuvers. Compared with the passive baseline, the NMPC controller reduces the semitrailer Load Transfer Ratio (LTR) and improves roll response in the main steering scenarios. These results indicate that, within the simulation environment and actuator constraints, the NMPC-based active air suspension strategy improves the roll stability of tractor-semitrailer combinations and provides a useful reference for future active suspension control in heavy-duty vehicles.

Keywords: active air suspension, nonlinear model predictive control, roll stability, tractor-semitrailer vehicle, load transfer ratio

Acknowledgements

First and foremost, we would like to express our deepest gratitude to Volvo Group Trucks Technology (GTT) for providing the opportunity to carry out this Master's thesis project. We are immensely grateful for the technical resources, office space, and the platform that made this research possible.

Special thanks go to our industrial supervisors, Esteban Gelso and Maliheh Sadeghi Kati. Their technical guidance and continued support were invaluable to the success of this work.

We would also like to extend our sincere appreciation to Nrupathunga Ashok for his valuable support and insights regarding the air suspension components, and to Berk Varol for his crucial assistance in resolving technical issues within the VTM model environment.

In addition, we would like to thank our academic examiner, Jonas Fredriksson, at the Department of Electrical Engineering, Chalmers University of Technology. Your rigorous academic feedback, constructive critiques, and expertise in control theory greatly elevated the quality and depth of this thesis.

Fanxiang Liao, Gothenburg, May 2026
Chaojie Lu, Gothenburg, May 2026

List of Acronyms

Below is the list of acronyms that have been used throughout this thesis listed in alphabetical order:

AYC	Active Yaw Control
CoG	Center of Gravity
ECAS	Electronically Controlled Air Suspension
ESC	Electronic Stability Control
HiL	Hardware-in-the-Loop
LCV	Longer Combination Vehicle
LTR	Load Transfer Ratio
MPC	Model Predictive Control
NMPC	Nonlinear Model Predictive Control
PID	Proportional-Integral-Derivative
RA	Rearward Amplification
SRT	Static Rollover Threshold
TCN	Temporal Convolutional Network
VTM	Volvo Transport Model

Nomenclature

Below is the nomenclature of indices, sets, parameters, and variables that have been used throughout this thesis.

Indices

i	Index for tire-suspension units (i = 1, . . . , 4)
k	Discrete time step index in NMPC horizon
t	simulation time

Parameters

m	Equivalent mass of the tractor
I_{xx}	Roll moment of inertia of the tractor body
I_{yy}	Pitch moment of inertia of the tractor body
I_{zz}	Yaw moment of inertia of the tractor body
h_c	Height of the center of gravity of the tractor body
R_C	Roll center height
h_r	Distance between the roll center and the center of gravity
h_{pitch}	Distance between the pitch center and the center of gravity
l_f	Longitudinal distance from the center of gravity to the front axle
l_r	Longitudinal distance from the center of gravity to the rear axle
l_H	Longitudinal distance from the center of gravity to the hitch point
h_H	Height of the hitch point
w_f	Front track width
w_r	Rear track width

w_{sf}	Half lateral spacing of the front suspension units
w_{sr}	Half lateral spacing of the rear suspension units
$D_{z,f}$	Equivalent vertical damping of the front suspension
$D_{z,r}$	Equivalent vertical damping of the rear suspension
$K_{\phi,f}$	Roll stiffness contribution of the front suspension
$K_{\phi,r}$	Roll stiffness contribution of the rear suspension
$D_{\phi,f}$	Roll damping contribution of the front suspension
$D_{\phi,r}$	Roll damping contribution of the rear suspension
R	Specific gas constant of air
T_s	Air temperature inside the air spring
$V_{0,f}$	Initial air spring volume of the front suspension
$V_{0,r}$	Initial air spring volume of the rear suspension
$A_{ef,f}$	Effective area of the front air spring
$A_{ef,r}$	Effective area of the rear air spring
g	Gravitational acceleration
η	Drivetrain efficiency
r	Effective wheel radius
C_d	Aerodynamic drag coefficient
A_f	Frontal area used in the aerodynamic drag model
ρ	Air density
C_{rr}	Rolling resistance coefficient

Variables

v_x	Longitudinal velocity
v_y	Lateral velocity
ψ	Yaw angle
$\dot{\psi}$	Yaw rate
$\ddot{\psi}$	Yaw acceleration
ϕ	Roll angle
$\dot{\phi}$	Roll rate
$\ddot{\phi}$	Roll acceleration
θ	Pitch angle
$\dot{\theta}$	Pitch rate

$\ddot{\theta}$	Pitch acceleration
z_i	Suspension deflection at corner i
$\dot{z}_i$	Suspension velocity
α_i	Slip angle of tire i
δ_i	Steering angle of front wheels
$F_{x,i}$	Longitudinal tire force
$F_{y,i}$	Lateral tire force
$F_{z,i}$	Vertical suspension force
$F_{z,\text{tire},i}$	Vertical tire load
F_x	Total longitudinal force
F_y	Total lateral force
F_{drag}	Aerodynamic drag force
F_{roll}	Rolling resistance force
F_{Hx}	Hitch longitudinal force
F_{Hy}	Hitch lateral force
F_{Hz}	Hitch vertical force
T_{Hx}	Hitch roll moment
M_X	Roll moment about longitudinal axis
M_Y	Pitch moment about lateral axis
M_Z	Yaw moment about vertical axis
P_i	Air spring pressure
$\dot{P}_i$	Pressure rate
$V_{s,i}$	Air spring volume
$\dot{V}_{s,i}$	Volume rate
$\dot{m}_{s,i}$	Air mass flow rate
$\dot{m}_{\text{in},i}$	Inflow mass rate
$\dot{m}_{\text{out},i}$	Outflow mass rate
$u_{v,i}$	Valve control signal
$\Delta F_{z,i}$	Suspension force increment
$\Delta \dot{F}_{z,i}$	Force increment rate
$\Delta F_z^\star$	Desired force increment
ν	Control input (force increment rate)

Contents

List of Acronyms **ix**

Nomenclature **xi**

List of Figures **xvii**

List of Tables **xix**

1 Introduction **1**
1.1 Background . . . 1
1.2 Related Work . . . 2
1.2.1 Articulated Vehicle Rollover Assessment and Threshold Prediction . . . 2
1.2.2 Air Suspension Modeling and Vehicle System Characterization 2
1.2.3 Evolution of Active Stability Control Strategies . . . 3
1.3 Problem Statement . . . 3
1.4 Objectives . . . 4
1.5 Scope and Limitations . . . 4

2 VTM Model and Suspension Extension Verification **7**
2.1 High-Fidelity VTM Plant . . . 7
2.2 Suspension Extension in the VTM . . . 7
2.2.1 Equivalent Suspension Parameters . . . 8
2.3 Verification of the Extended VTM Model . . . 9
2.3.1 Verification under Steering Maneuver . . . 9
2.3.2 Verification under Straight-Line Braking . . . 10
2.3.3 Summary of Verification Cases . . . 11
2.4 Air Spring Modeling . . . 11

3 Two-Track Modeling of the Tractor-Semitrailer Combination **15**
3.1 Model Structure and State Selection . . . 15
3.1.1 Modeling Assumptions . . . 16
3.2 Vehicle and Suspension Parameters . . . 17
3.3 Longitudinal Dynamics . . . 18
3.4 Vertical Dynamics . . . 19
3.5 Lateral Dynamics . . . 21
3.6 Yaw Dynamics . . . 23

3.7 Roll Dynamics . . . 23
3.8 Pitch Dynamics . . . 24
3.9 Validation Against the VTM Model . . . 25
3.9.1 Validation under Step Steering Input . . . 25
3.9.2 Validation under Straight-Line Braking . . . 25
3.9.3 Summary of Validation Cases . . . 26

4 Controller Design **29**
4.1 Control Objectives . . . 29
4.2 Control Architecture . . . 29
4.3 Controller Variables and Layer Interfaces . . . 31
4.4 Trailer Preview Treatment . . . 32
4.5 Upper-layer NMPC Controller . . . 33
4.5.1 Prediction Model . . . 33
4.5.2 Numerical Settings . . . 34
4.5.3 Cost Function . . . 34
4.5.4 Constraints . . . 36
4.6 Force-to-Pressure Allocation . . . 37
4.7 Pressure Tracking and Valve Logic . . . 37
4.8 Baseline Controllers . . . 38

5 Simulation Setup and Evaluation Metrics **39**
5.1 Vehicle and Controller Cases . . . 39
5.2 Test Maneuvers . . . 39
5.3 Evaluation Metrics . . . 40

6 Results and Analysis **43**
6.1 Roll and Load Transfer Response . . . 43
6.1.1 Step Steering Transient Response . . . 43
6.1.2 Ramp Steering Response . . . 44
6.1.3 Directional Reversal: Lane Change . . . 46
6.1.4 Slow Lane Change . . . 47
6.1.5 Coupled Dynamics: Braking While Steering . . . 48
6.2 Stability Boundary and LTR Surface . . . 49
6.3 Handling Response and Trailer Rearward Behavior . . . 51
6.4 Trajectory and Braking Distance . . . 52
6.5 Overall Discussion . . . 54

7 Conclusions and Future Work **57**
7.1 Conclusion . . . 57
7.2 Future Work . . . 57

Bibliography **59**

List of Figures

2.1 Suspension extension in the VTM 8
2.2 VTM roll comparison 10
2.3 VTM pitch comparison 10

3.1 Two-track model top view 18
3.2 Two-track model front view 20
3.3 Two-track model side view 22
3.4 Step steering validation 25
3.5 Straight braking validation 26

4.1 Active suspension controller structure. 30
4.2 Hitch Force and Moment Transformation 32

6.1 Step steering input 43
6.2 LTR response under step steering 44
6.3 Roll response under step steering 44
6.4 Ramp steering input 45
6.5 LTR response under ramp steering 45
6.6 Roll response under ramp steering 45
6.7 Lane-change input 46
6.8 Lane-change LTR comparison 46
6.9 Lane-change roll comparison 47
6.10 Slow lane-change input 47
6.11 Slow lane-change responses 48
6.12 Steering-braking response comparison 49
6.13 LTR surface comparison 50
6.14 LTR boundary shift 50
6.15 Understeer-gradient comparison 51
6.16 Trailer acceleration response 52
6.17 Step and ramp trajectories 53
6.18 Lane-change trajectory 53
6.19 Stopping distance comparison 54

List of Tables

2.1 VTM validation matrix 11

3.1 Control-oriented states 16
3.2 Suspension-force inputs 16
3.3 Vehicle model parameters and their modeling roles. 17
3.4 Error metrics for the mathematical-model validation cases. 27

4.1 Controller layer interfaces 31
4.2 NMPC numerical settings 34
4.3 NMPC weighting terms 35
4.4 Pressure controller thresholds 38

5.1 Current closed-loop comparison cases. 40

6.1 LTR trade-off summary 46
6.2 Rearward amplification summary 52
6.3 NMPC result summary 54

1

Introduction

1.1 Background

Road freight transportation plays an essential role in global supply chains and industrial logistics. In the heavy-duty commercial transport sector, articulated vehicle combinations, especially tractor-semitrailer configurations, are widely used because they offer high payload capacity and efficient transport within legal axle-load limits. However, their large dimensions, high gross weights, and articulated mechanical structures also lead to strong multi-body coupling and nonlinear vehicle dynamics, which can create serious safety challenges during operation [1]. According to global traffic safety statistics, rollover accidents account for a considerable proportion of severe heavy commercial vehicle crashes and are often associated with high fatality rates and significant economic losses. To reduce these risks, regulatory guidelines such as the *Heavy Vehicle Stability Guide* define requirements for the Static Rollover Threshold (SRT) and the dynamic handling performance of heavy-duty vehicle combinations [2].

From the perspective of multi-body system dynamics, heavy articulated vehicles typically have a relatively high center of gravity (CoG) and experience large payload variations. As a result, their passive roll stability margins are generally lower than those of single-unit passenger vehicles. Winkler et al. [3] showed that loaded heavy vehicles can reach rollover within their normal or emergency maneuvering range. In addition, the fifth-wheel connection between the tractor and semitrailer introduces strong lateral-roll coupling. During transient steering maneuvers, including lane changes, roundabout driving, and obstacle avoidance, the trailing unit may exhibit rearward amplification [4, 5]. The trailer response can therefore become more critical than the tractor response. Kharrazi [7] also showed that lateral motion can be amplified through the towed units of longer vehicle combinations.

In real-world operation, rollover risk can be further increased by asymmetric cargo distribution and load shifting [8]. The vehicle center of mass can move away from the longitudinal centerline and reduce the available roll margin. Therefore, an active actuator system and a suitable control strategy are needed to reduce roll motion while retaining the suspension's normal support function [9, 10].

1.2 Related Work

To reduce rollover risks in heavy articulated vehicles, previous studies have mainly focused on three related aspects: roll stability assessment, air suspension and vehicle system modeling, and active stability control strategies. These studies provide the theoretical and technical basis for developing predictive roll control methods for tractor-semitrailer combinations.

1.2.1 Articulated Vehicle Rollover Assessment and Threshold Prediction

Accurate assessment of roll stability is an important basis for active safety intervention. Existing studies have investigated rollover limits through threshold mapping, warning methods, and trajectory constraints. Hung [4] used simulation to study dynamic rollover thresholds of tractor-semitrailer combinations under steering inputs. Hung and Khanh [11] presented a multibody method for determining dynamic warning and control thresholds. For autonomous evasive maneuvers, Anistratov [12] studied vehicle stability within a trajectory-optimization problem. Future vehicle motion can also be estimated from data. Azadani and Boukerche [13] proposed a multimodal path-prediction method based on temporal convolutional networks. Such a method can provide preview information, although it does not directly solve the suspension-control problem.

1.2.2 Air Suspension Modeling and Vehicle System Characterization

Among different active chassis actuators, active air suspension is a practical solution for heavy commercial vehicles because it offers adjustable pneumatic stiffness, variable damping characteristics, and chassis height regulation over a wide operating range [14, 10]. However, accurate modeling of pneumatic air springs remains challenging due to the coupled thermodynamic and mechanical nonlinearities of the air spring system.

For vehicle-level modeling, the multibody framework described by Shabana [15] provides a basis for articulated mechanical systems. Nieto et al. [16] developed an analytical pneumatic-suspension model from experimental characterization. Chen et al. [17] studied how balanced airflow in heavy-truck air suspension affects roll response. Larten [14] addressed modeling and parameter identification for heavy-duty air suspension. Sun et al. [18] presented a hybrid approach for electronically controlled air-suspension height adjustment. The Volvo Transport Model and its supporting documentation provide the high-fidelity simulation plant used in this work [19, 20].

1.2.3 Evolution of Active Stability Control Strategies

Early active safety systems for heavy vehicles mainly focused on planar yaw stability. Typical approaches include active yaw control, electronic stability control, differential braking, and active steering [21]. These methods can improve directional stability, but roll motion also needs direct attention in a high-CoG vehicle. Cho et al. [22] used semi-active dampers to coordinate yaw, roll, and pitch motion. Ricco et al. [23] developed an NMPC framework for yaw rate and body-motion control through semi-active and active suspensions.

Suspension-based roll control can directly influence load transfer and body roll. Chen et al. [24] showed that pneumatic air management can produce an anti-roll-bar effect. Sampson [25] studied active roll control for articulated heavy vehicles, and Sampson and Cebon [9] analyzed the achievable roll-stability limits. Miege and Cebon [26] developed and validated an optimal roll-control model for an articulated vehicle. More recently, Lee and Olsson [10] implemented active air suspension and NMPC for heavy-vehicle roll stability.

Advanced control algorithms have also been studied for active suspension and roll stability. Gaspar et al. [27] used an LPV method to improve rollover stability with active suspension. Vu et al. [6] used LQR control with an active hydraulic anti-roll bar. MPC is useful when actuator limits and multiple control objectives must be addressed simultaneously. Sun et al. [28] applied MPC to an air-suspension system represented by a hybrid model. Jeong [29] combined path tracking and rollover prevention in an MPC framework for an articulated electric vehicle. Zhou et al. [30] proposed cooperative MPC for interconnected air suspension. Yim [31] developed a preview controller that uses future path information for rollover prevention.

Overall, existing studies have shown the potential of active air suspension, robust control, MPC, and preview control for improving roll stability. The previous thesis by Lee and Olsson established an air-spring model and an NMPC framework for a heavy vehicle without the semitrailer configuration used here [10]. The present work starts from that framework. It adapts the plant and controller to a tractor–semitrailer combination and revises how pneumatic limits are handled inside the controller.

1.3 Problem Statement

The earlier controller framework was developed without the tractor–semitrailer coupling used in this thesis [10]. It also represented part of the pneumatic actuator behavior by fixing mass-flow-related quantities inside the controller model. This can prescribe force development that is not consistent with the current air-spring pressure and valve operating point.

The problem addressed in this thesis is therefore to adapt and reformulate that framework for a 4x2-axle tractor connected to a passive three-axle semitrailer. The

controller needs a mathematical prediction model to estimate future vehicle motion and suspension force demand. This model must include the tractor's main roll and pitch motions and the loads transmitted through the fifth wheel. It must also describe the available pneumatic actuation without placing the full air-spring pressure and mass-flow dynamics inside the vehicle prediction model.

The adopted solution separates vehicle prediction from pneumatic actuation. The nonlinear vehicle model predicts longitudinal, lateral, yaw, roll, and pitch motion. The semitrailer influence is represented by measured hitch forces and moments, as well as by a bounded coupling-preview term. Air-suspension pressure and flow limits are handled through force and force-rate constraints and through the lower pressure-control layer. The VTM remains the Simscape plant used to evaluate the complete tractor–semitrailer response.

1.4 Objectives

The objectives of the thesis are:

- to prepare and verify a VTM model consisting of a 4x2 tractor and a three-axle semitrailer,
- to extend the tractor suspension so that the left and right air-spring forces can be controlled independently while the semitrailer remains passive,
- to reformulate the previous control-oriented model by adding pitch dynamics and tractor–semitrailer hitch coupling,
- to replace fixed mass-flow behavior in the controller model with physical force, force-rate, pressure, and mass-flow related limits,
- to compare the passive suspension, a height-based PID controller, and the revised NMPC under steering and braking maneuvers,
- to evaluate roll angle, pitch angle, load transfer ratio, lateral acceleration, rearward amplification, and trajectory response.

1.5 Scope and Limitations

Since this thesis focuses on the development and simulation-based evaluation of a predictive controller for active air suspension, several limitations are considered:

- **Simulation-only validation:** The controller is evaluated only in a simulation environment based on the VTM. No hardware test, field experiment, or full-scale vehicle validation is performed.
- **Assumed preview information:** Future steering inputs are assumed to be available to the controller. In a real vehicle implementation, such preview information would require additional sensing, path prediction, or driver-intention estimation.
- **No state observer included:** The controller assumes that the required vehicle states are available from the simulation environment. State estimation and observer design are not included in this thesis.

- **Limited road and load uncertainty:** Variations in road friction, road unevenness, wind disturbance, and dynamic cargo movement are not explicitly modeled. The analysis therefore focuses on predefined simulation conditions.
- **Research prototype implementation:** The controller is implemented in MATLAB/Simulink with CasADi and IPOPT. Code generation, move blocking, solver acceleration, and real-time deployment are outside the scope of this thesis.

2

VTM Model and Suspension Extension Verification

The chapter then verifies the extended model against the original VTM and summarizes the air-spring representation used for the active suspension system.

2.1 High-Fidelity VTM Plant

The Volvo Transport Model (VTM) is used as the high-fidelity simulation plant in this thesis. The plant represents a 4x2 tractor connected to a three-axle semitrailer and includes nonlinear multibody dynamics, suspension behavior, tire-force generation, braking response, and mechanical coupling through the fifth wheel. It therefore provides the reference environment for evaluating vehicle responses under steering and braking maneuvers.

The VTM is separate from the reduced-order prediction model used inside the NMPC. In the simulations, the VTM generates the vehicle response for the passive suspension, the PID-controlled suspension, and the NMPC-controlled suspension. Using the same plant for all controller variants makes the comparison dependent on the suspension-control strategy rather than on changes in the vehicle model.

The original VTM plant represents the suspension at an axle level and is primarily suited for passive vehicle-response simulation. Active roll control requires independent left and right vertical-force inputs on the tractor suspension. The suspension interface used to provide these inputs is introduced in the following section.

2.2 Suspension Extension in the VTM

The original VTM suspension interface is extended to allow the left and right suspension actions to be represented separately. In the original representation, the suspension action of an axle is mainly described through an equivalent vertical stiffness and damping together with roll-related stiffness and damping. This is sufficient to reproduce the passive vehicle behavior, but it does not provide a direct actuation path to apply different vertical forces on the left and right sides.

For active roll control, the controller must be able to increase vertical support on one side of the tractor and decrease it on the other. Therefore, the axle-level suspension representation is replaced with two lateral suspension paths, one on the left and one on the right. Each side has its own vertical suspension action, while the original body, axle, tire, and fifth-wheel structures are kept unchanged. The semitrailer suspension model is not modified and remains passive in all simulations.

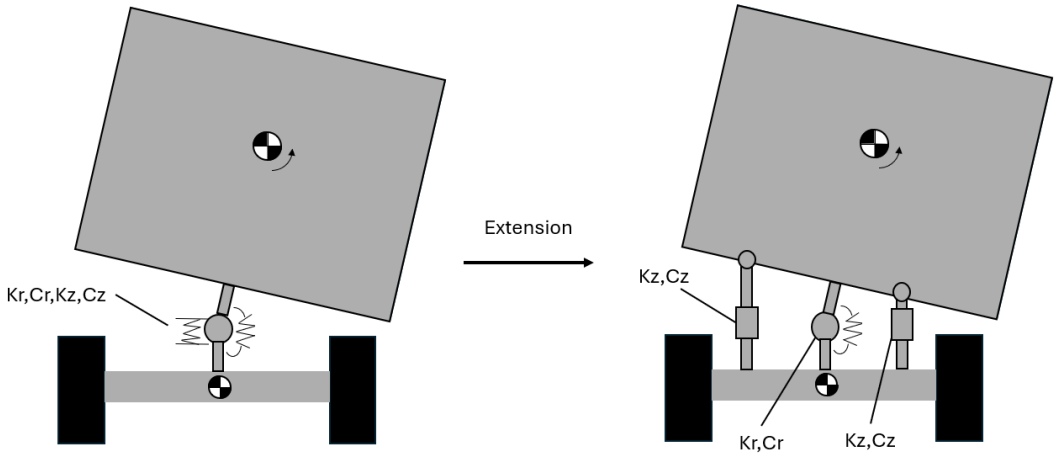

Figure 2.1: Suspension extension in the VTM

Figure 2.1 illustrates the basic idea of the suspension extension. In the original model, the suspension behavior is represented by an equivalent axle-level structure. After the extension, the vertical suspension paths are separated into left and right sides. The equivalent stiffness and damping parameters are selected so that the passive response of the extended model remains close to that of the original VTM model when no active left-right force difference is applied.

The extended model is compared with the original passive VTM model before controller evaluation to quantify the response changes introduced by the suspension interface.

2.2.1 Equivalent Suspension Parameters

The parameter definitions follow the notation in Fig. 2.1, and the conversion method follows Lee and Olsson [10]The original axle-level vertical stiffness and damping are divided between the left and right suspension paths:

$$K_z = \frac{K_{z,\mathrm{vtm}}}{2}, \qquad C_z = \frac{C_{z,\mathrm{vtm}}}{2}, \tag{2.1}$$

where $K_{z,\mathrm{vtm}}$ and $C_{z,\mathrm{vtm}}$ are the original VTM axle-level vertical stiffness and damping. In the extended model, the axle is represented by separate left- and right-side

suspension elements. Therefore, half of the original axle-level stiffness and damping is assigned to each side, giving the single-side parameters K_z and C_z. Where K_r denotes the equivalent passive roll stiffness, while C_r denotes the equivalent passive roll damping. These terms describe the roll resistance that is not represented directly by the left and right vertical suspension paths. The suspension extension itself only requires the conversion of K_z and C_z given above.

2.3 Verification of the Extended VTM Model

The verification procedure evaluates whether the suspension extension changes the passive response of the original VTM plant. The original and extended models use the same vehicle configuration, road condition, initial state, steering input, and braking input. Active control is disabled in both models.

Six different tests with increasing levels of challenge were conducted. All tests use MATLAB R2020b. First, three step steering tests at 10 m/s with amplitudes of 0.05, 0.10, and 0.15 rad were performed. Then, three straight-line braking tests were performed from 8, 10, and 12 m/s. Braking starts at $t = 2$ s and each simulation is stopped when $|v_x| \leq 0.05$ m/s. Two representative results are shown, while all six errors are reported in Table 2.1.

Note that for easier comparison between the original and extended models, the pre-input mean value is removed from each signal, so the models start from the same attitude. No scaling or time shifting is applied.

The difference between the original and extended models is evaluated using the time-domain error

$$e_x(t) = x_{\text{ext}}(t) - x_{\text{ori}}(t), \tag{2.2}$$

where $x_{\text{ext}}(t)$ is the response of the extended VTM model and $x_{\text{ori}}(t)$ is the response of the original VTM model. The mean error, root mean square error (RMSE), and maximum absolute error are used to quantify the difference between the two models:

$$\bar{e}_x = \frac{1}{N_s} \sum_{j=1}^{N_s} e_x(t_j), \tag{2.3}$$

$$e_{\text{RMSE}} = \sqrt{\frac{1}{N_s} \sum_{j=1}^{N_s} e_x^2(t_j)}, \tag{2.4}$$

$$e_{\max} = \max_j \left| e_x(t_j) \right|, \tag{2.5}$$

where N_s is the number of sampled time points used in the comparison.

2.3.1 Verification under Steering Maneuver

The steering maneuver is used to verify the roll behavior of the extended suspension model. Figure 2.2 shows the representative 0.10 rad case. The steering command

starts at $t = 2$ s and uses a 0.25 s smoothing interval to avoid a numerical discontinuity.

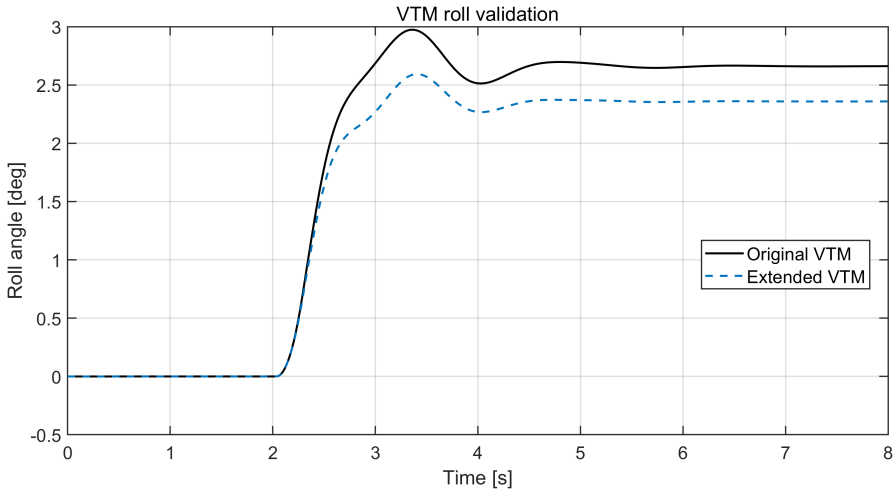

Figure 2.2: VTM roll comparison

The extended model follows the rise time and oscillation pattern of the original VTM, but its roll magnitude is lower. In the representative case, the RMSE is 0.259°, and the maximum absolute error is 0.425°. The difference grows as the steering input increases. The suspension extension retains the main roll trend but does not exactly reproduce the original passive roll amplitude.

2.3.2 Verification under Straight-Line Braking

The straight-line braking case checks the pitch behavior. Figure 2.3 shows the representative test from 10 m/s. The same wheel-brake demand is applied to both models, and the comparison ends when the vehicle reaches the stopping threshold.

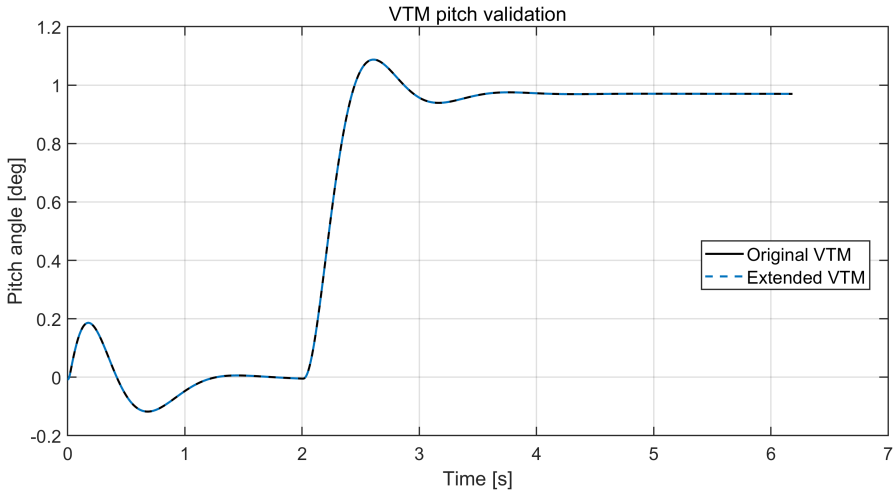

Figure 2.3: VTM pitch comparison

The two pitch curves are almost identical. At 10 m/s, the pitch RMSE is 3.62×10^{-6} °

and the maximum absolute error is 3.95×10^{-5} °. The stopping times are also nearly equal. They are approximately 5.34, 6.18, and 7.03 s for the 8, 10, and 12 m/s tests.

2.3.3 Summary of Verification Cases

The six verification cases described above are summarized in Table 2.1. The steering input amplitude is varied to examine the roll response at different lateral excitation levels, while the initial vehicle speed is varied in the braking tests to evaluate the consistency of the pitch response. The table summarizes the mean error, root-mean-square error (RMSE), and maximum absolute error for all completed verification cases. Since the corresponding time-domain responses exhibit similar trends to those presented in the previous section, the additional plots are omitted.

Test	Input	Response	Mean [deg]	RMSE [deg]	Max. error [deg]
Step steering	0.05 rad	Roll	−0.106989	0.129367	0.219167
Step steering	0.10 rad	Roll	−0.214629	0.258715	0.425204
Step steering	0.15 rad	Roll	−0.323383	0.388556	0.608066
Braking	8 m/s	Pitch	-7.67×10^{-7}	3.15×10^{-6}	3.95×10^{-5}
Braking	10 m/s	Pitch	-9.15×10^{-7}	3.62×10^{-6}	3.95×10^{-5}
Braking	12 m/s	Pitch	4.42×10^{-7}	5.15×10^{-6}	3.19×10^{-5}

Table 2.1: VTM validation matrix

The braking cases show very small pitch errors across the tested speed range, indicating that the longitudinal load-transfer and pitch characteristics of the original model are effectively preserved after the suspension extension. No clear increase in the pitch error is observed as the initial speed increases from 8 to 12 m/s.

For the steering cases, the extended model reproduces the overall roll-response trend, although the negative mean errors indicate that its roll magnitude is systematically lower than that of the original model. Both the RMSE and maximum error increase approximately with the steering input amplitude, suggesting that the discrepancy becomes more pronounced under stronger lateral excitation. Nevertheless, the response remains consistent in direction and general dynamic behavior.

Overall, the verification results indicate that the suspension extension preserves the main pitch and roll characteristics required for the subsequent controller development. The observed slight underestimation of roll magnitude represents a limitation of the extended passive model.

2.4 Air Spring Modeling

The active suspension model uses the air-spring formulation inherited from Lee and Olsson [10]. The pressure, force, and valve-flow equations follow established pneumatic suspension models [14, 16, 18]. The controller reformulation presented later changes how the actuator limits are imposed, while the underlying air-spring equations remain unchanged.

The pressure dynamics are derived from the ideal gas law [14, 24]. For an air spring chamber, the pressure rate can be written as

$$\dot{P}_{s,i} = \frac{P_{s,i}}{T_s}\dot{T}_s + \frac{RT_s}{V_{s,i}}\dot{m}_{s,i} - \frac{P_{s,i}}{V_{s,i}}\dot{V}_{s,i}, \tag{2.6}$$

where $P_{s,i}$ is the absolute pressure inside air spring i, T_s is the air temperature, R is the specific gas constant of air, $V_{s,i}$ is the air spring volume, and $\dot{m}_{s,i}$ is the mass flow rate into or out of the air spring.

The temperature inside the air spring is assumed to be constant, i.e., $\dot{T}_s = 0$. The air spring volume is assumed to vary linearly with the local suspension deflection. With the sign convention used, the change in volume can be written as

$$V_{s,i} = V_{0,i} + A_{\text{eff},i} z_i, \tag{2.7}$$

or as

$$\dot{V}_{s,i} = A_{\text{eff},i} \dot{z}_i. \tag{2.8}$$

where $V_{0,i}$ is the nominal air spring volume, $A_{\text{eff},i}$ is the effective air spring area, and z_i is the local suspension deflection. With this convention, positive z_i corresponds to an increase of the air spring volume. Substituting Eqs. (2.7) and (2.8) into Eq. (2.6) gives

$$\dot{P}_{s,i} = \frac{RT_s}{V_{0,i} + A_{\text{eff},i} z_i}\dot{m}_{s,i} - \frac{P_{s,i} A_{\text{eff},i}}{V_{0,i} + A_{\text{eff},i} z_i}\dot{z}_i. \tag{2.9}$$

The vertical force generated by the air spring is calculated from the pressure difference across the air spring and the effective area:

$$F^p_{z,i} = (P_{s,i} - P_{\text{atm}})\, A_{\text{eff},i}, \tag{2.10}$$

where P_{atm} is the atmospheric pressure. In the implementation, this pressure-based force is combined with the suspension damping contribution when the total vertical suspension force is applied to the VTM plant.

The static preload pressure is selected so that the air spring balances the nominal static load. For one side of an axle, this gives

$$F_{0,i} = (P_{0,i} - P_{\text{atm}})\, A_{\text{eff},i}, \tag{2.11}$$

and therefore

$$P_{0,i} = \frac{F_{0,i}}{A_{\text{eff},i}} + P_{\text{atm}}. \tag{2.12}$$

This pressure is used as the nominal pressure around which the active pressure variation is generated.

The air mass flow is determined by the on–off valve state. The valve connects the air spring to the supply tank, the atmosphere, or neither. The choked and unchoked flow expressions follow the model used in the previous thesis and the cited air-suspension

literature [10, 24, 18]. For a general upstream pressure p_u and downstream pressure p_d, the mass flow magnitude is

$$\dot{m}_s = \begin{cases} s\dfrac{p_u}{\sqrt{RT_s}}\sqrt{\gamma\left(\dfrac{2}{\gamma+1}\right)^{\frac{\gamma+1}{\gamma-1}}}, & 0 < \dfrac{p_d}{p_u} \le b, \\ s\sqrt{\dfrac{2}{RT_s}}\sqrt{p_d(p_u - p_d)}, & b < \dfrac{p_d}{p_u} \le 1, \end{cases} \tag{2.13}$$

where s is the effective valve flow area, γ is the specific heat ratio of air, and b is the critical pressure ratio.

During filling, the upstream pressure is the tank pressure P_{tank} and the downstream pressure is the air spring pressure $P_{s,i}$. The inflow becomes

$$\dot{m}_{\text{in},i} = \begin{cases} s\dfrac{P_{\text{tank}}}{\sqrt{RT_s}}\sqrt{\gamma\left(\dfrac{2}{\gamma+1}\right)^{\frac{\gamma+1}{\gamma-1}}}, & 0 < \dfrac{P_{s,i}}{P_{\text{tank}}} \le b, \\ s\sqrt{\dfrac{2}{RT_s}}\sqrt{P_{s,i}(P_{\text{tank}} - P_{s,i})}, & b < \dfrac{P_{s,i}}{P_{\text{tank}}} \le 1. \end{cases} \tag{2.14}$$

During venting, the upstream pressure is the air spring pressure $P_{s,i}$ and the downstream pressure is the atmospheric pressure P_{atm}. The outflow is written as a negative mass flow into the air spring:

$$\dot{m}_{\text{out},i} = \begin{cases} -s\dfrac{P_{s,i}}{\sqrt{RT_s}}\sqrt{\gamma\left(\dfrac{2}{\gamma+1}\right)^{\frac{\gamma+1}{\gamma-1}}}, & 0 < \dfrac{P_{\text{atm}}}{P_{s,i}} \le b, \\ -s\sqrt{\dfrac{2}{RT_s}}\sqrt{P_{\text{atm}}(P_{s,i} - P_{\text{atm}})}, & b < \dfrac{P_{\text{atm}}}{P_{s,i}} \le 1. \end{cases} \tag{2.15}$$

The valve command signal, $u_{v,i}$, controls the mass flow used in Eq. (2.9), according to

$$\dot{m}_{s,i} = \begin{cases} \dot{m}_{\text{in},i}, & u_{v,i} > d_z, \\ 0, & |u_{v,i}| \le d_z, \\ \dot{m}_{\text{out},i}, & u_{v,i} < -d_z, \end{cases} \tag{2.16}$$

where $u_{v,i}$ is the valve command and d_z is the valve dead zone. Thus, a positive valve command fills the air spring, a negative command vents the air spring, and a command inside the dead zone keeps the valve closed.

Equations (2.9)–(2.16) describe the pressure-force and mass-flow behavior used by the lower-level air suspension actuation model. In the controller architecture introduced later, the upper-layer controller computes desired vertical force increments, the allocation layer converts these force requests into pressure references, and the valve logic determines whether each air spring should be filled, held, or vented.

3

Two-Track Modeling of the Tractor-Semitrailer Combination

This chapter presents the control-oriented two-track model used for NMPC prediction. The model describes the tractor translational and rotational dynamics, while the semitrailer influence is represented through forces and moments transmitted at the fifth wheel. The chapter defines the state and input variables, coordinate and sign conventions, vehicle and suspension parameters, equations of motion, and validation against the high-fidelity VTM plant.

3.1 Model Structure and State Selection

The controller requires a mathematical model to predict how the vehicle will respond to steering, braking, hitch loads, and changes in suspension forces. A nonlinear two-track model is used for this purpose. The formulation follows standard vehicle-dynamics modeling and the optimization-oriented vehicle model presented by Anistratov [1, 12].

The model is formulated in the tractor body-fixed coordinate system. The x-axis points forward, the y-axis points to the left, and the z-axis points upward. Positive roll angle ϕ is defined about the x-axis, positive pitch angle θ about the y-axis, and positive yaw angle ψ about the z-axis, all following the right-hand rule. Tire and fifth-wheel coupling effects are represented through force and moment terms. Four suspension-force increments act on the tractor body as external control forces. Air pressure and mass flow are not vehicle-model states. Their limits are introduced later in the controller constraints and lower-level actuation model. The vehicle states are summarized in Table 3.1.

State	Description
v_x	Longitudinal velocity of the tractor
v_y	Lateral velocity of the tractor
ψ	Yaw angle of the tractor body
$\dot{\psi}$	Yaw rate of the tractor body
ϕ	Roll angle of the tractor body
$\dot{\phi}$	Roll rate of the tractor body
θ	Pitch angle of the tractor body
$\dot{\theta}$	Pitch rate of the tractor body

Table 3.1: Control-oriented states

The suspension-force inputs are summarized in Table 3.2. Their rates are introduced as decision variables in Chapter 4.

Input	Description
$\Delta F_{z,FL}$	Front-left suspension force increment
$\Delta F_{z,FR}$	Front-right suspension force increment
$\Delta F_{z,RL}$	Rear-left suspension force increment
$\Delta F_{z,RR}$	Rear-right suspension force increment

Table 3.2: Suspension-force inputs

The NMPC does not directly optimize valve commands or air mass flow; it optimizes the force increments over the prediction horizon. The resulting force requests are converted into pressure references and valve commands by the lower-level modules.

3.1.1 Modeling Assumptions

The following assumptions are adopted in the control-oriented modeling:

1. The tractor body is treated as a rigid body.
2. The trailer influence on the tractor is represented through hitch-transmitted forces and moments.
3. Vertical body heave is not modeled as an independent degree of freedom.
4. Tire forces are described by a nonlinear tire model parameterized by slip angle and normal load.
5. Future steering angles are assumed to be known over the prediction horizon.
6. The required vehicle states are assumed to be available from the VTM model, and no state observer is considered.
7. The road is flat, and road-bank and road-slope angles are not included.

These assumptions keep the model focused on the tractor motion required for NMPC prediction, while excluding heave, observer design, road-bank effects, and detailed pneumatic states from the vehicle equations.

3.2 Vehicle and Suspension Parameters

This section summarizes the principal vehicle and suspension parameters used in the tractor model. These parameters describe the mass and inertia properties of the tractor body, the geometric locations of the axles, suspension units, and hitch point, and the effective properties of the active air suspension system.

Due to confidentiality restrictions, the exact numerical values of several vehicle-specific parameters cannot be disclosed. However, the parameter symbols, physical units, and modeling roles are retained in order to preserve the structure of the formulation. The main parameters are listed in Table 3.3.

Parameter	Unit	Modeling role
m	kg	Tractor sprung mass
I_{xx}	$\mathrm{kg\,m^2}$	Roll moment of inertia
I_{yy}	$\mathrm{kg\,m^2}$	Pitch moment of inertia
I_{zz}	$\mathrm{kg\,m^2}$	Yaw moment of inertia
h_c	m	Center-of-gravity height
R_C	m	Roll-center geometry parameter
h_r	m	Roll-center height
h_{pitch}	m	Pitch moment arm
l_f	m	Distance from CoG to front axle
l_r	m	Distance from CoG to rear axle
l_H	m	Longitudinal hitch position
h_H	m	Hitch height
w_f	m	Front track width
w_r	m	Rear track width
w_{sf}	m	Front suspension half-spacing
w_{sr}	m	Rear suspension half-spacing
$D_{z,f}$	N s/m	Equivalent front vertical damping
$D_{z,r}$	N s/m	Equivalent rear vertical damping
$K_{\phi,T}$	N m/rad	Tractor roll stiffness
$D_{\phi,T}$	N m s/rad	Tractor roll damping
D_θ	N m s/rad	Pitch damping
$m_{u,f}$	kg	Front unsprung mass contribution
$m_{u,r}$	kg	Rear unsprung mass contribution
η	–	Drivetrain efficiency
r	m	Effective wheel radius
C_d	–	Aerodynamic drag coefficient
A_f	$\mathrm{m^2}$	Vehicle frontal area
ρ	$\mathrm{kg/m^3}$	Air density
C_{rr}	–	Rolling-resistance coefficient
g	$\mathrm{m/s^2}$	Gravitational acceleration

Table 3.3: Vehicle model parameters and their modeling roles.

3.3 Longitudinal Dynamics

The longitudinal dynamics describe the tractor's motion along its body-fixed longitudinal axis. The formulation follows Newton's second law in a moving body frame [1, 12]. Driving and braking forces, aerodynamic drag, rolling resistance, body-motion coupling, and the longitudinal reaction force at the fifth-wheel coupling point are included.

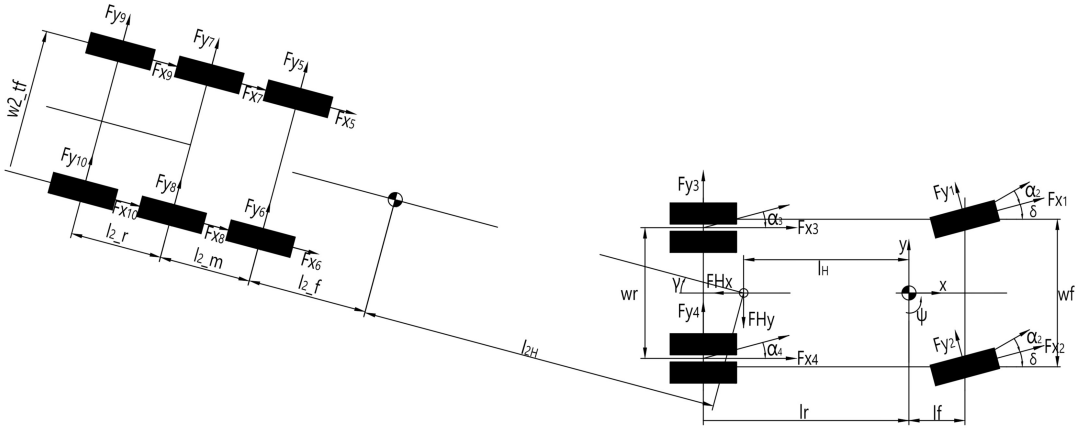

Figure 3.1: Two-track model top view

Figure 3.1 defines the axle positions, track widths, steering angles, and hitch location used in the longitudinal, lateral, and yaw equations. The signed longitudinal force generated at wheel i is expressed as

$$F_{x,i} = \frac{T_i \eta}{r_i}, \qquad i = 1, 2, 3, 4, \tag{3.1}$$

where T_i is the applied wheel torque, η is the drivetrain efficiency, and r_i is the effective wheel radius. The aerodynamic drag force is written as

$$F_{\text{drag}} = \frac{1}{2} \rho C_d A_f v_x^2, \tag{3.2}$$

where ρ is the air density, C_d is the aerodynamic drag coefficient, A_f is the frontal area, and v_x is the longitudinal velocity.

The rolling resistance force is written as

$$F_{\text{roll}} = C_{rr} m g, \tag{3.3}$$

where C_{rr} is the rolling resistance coefficient, m is the tractor mass, and g is the gravitational acceleration.

Taking the steering angles of the front wheels into account, the net longitudinal force acting on the tractor body is

$$\begin{aligned} F_x = \; & (F_{x1}\cos\delta_1 - F_{y1}\sin\delta_1) + (F_{x2}\cos\delta_2 - F_{y2}\sin\delta_2) \\ & + F_{x3} + F_{x4} - F_{\text{drag}} - F_{\text{roll}} - F_{Hx}, \end{aligned} \tag{3.4}$$

where δ_1 and δ_2 are the steering angles of the left and right front wheels, respectively, F_{y1} and F_{y2} are the front lateral tire forces, and F_{Hx} is the hitch-transmitted longitudinal force.

The longitudinal acceleration is then given by

$$\begin{aligned} \dot{v}_x = \; & \frac{F_x}{m} + v_y\dot{\psi} \\ & + h_{\text{pitch}}\Big(\sin\theta\cos\phi\left(\dot{\psi}^2 + \dot{\phi}^2 + \dot{\theta}^2\right) - \sin\psi\,\ddot{\psi} - 2\cos\psi\,\dot{\phi}\dot{\psi} \\ & \quad - \cos\theta\cos\phi\,\ddot{\theta} + 2\cos\theta\sin\phi\,\dot{\theta}\dot{\phi} + \sin\theta\sin\phi\,\ddot{\phi}\Big). \end{aligned} \tag{3.5}$$

The first term corresponds to the net longitudinal force, while $v_y\dot{\psi}$ represents the kinematic coupling introduced by the body-fixed coordinate system. The remaining terms account for the nonlinear coupling among the tractor body's yaw, roll, and pitch motions.

3.4 Vertical Dynamics

The vertical behavior of the tractor body is not modeled as an independent heave degree of freedom. Suspension deflection is obtained from roll and pitch motion. Four commanded suspension-force increments act on the tractor body. Air pressure, chamber volume, valve state, and mass flow are not states of this vehicle model.

Figure 3.2 shows the roll geometry and the left-right suspension-force locations. The vertical displacement of each suspension unit is determined by the tractor body's roll and pitch motion. Here, $i = 1, 2$ denotes the front axle and $i = 3, 4$ denotes the rear axle. The suspension deflections are expressed as

$$z_1 = w_{sf}\tan\phi - l_f\tan\theta, \tag{3.6}$$

$$z_2 = -w_{sf}\tan\phi - l_f\tan\theta, \tag{3.7}$$

$$z_3 = w_{sr}\tan\phi + l_r\tan\theta, \tag{3.8}$$

$$z_4 = -w_{sr}\tan\phi + l_r\tan\theta, \tag{3.9}$$

where w_{sf} and w_{sr} are the half lateral spacings of the front and rear suspension units, respectively, and l_f and l_r are the longitudinal distances from the center of gravity to the front and rear axles.

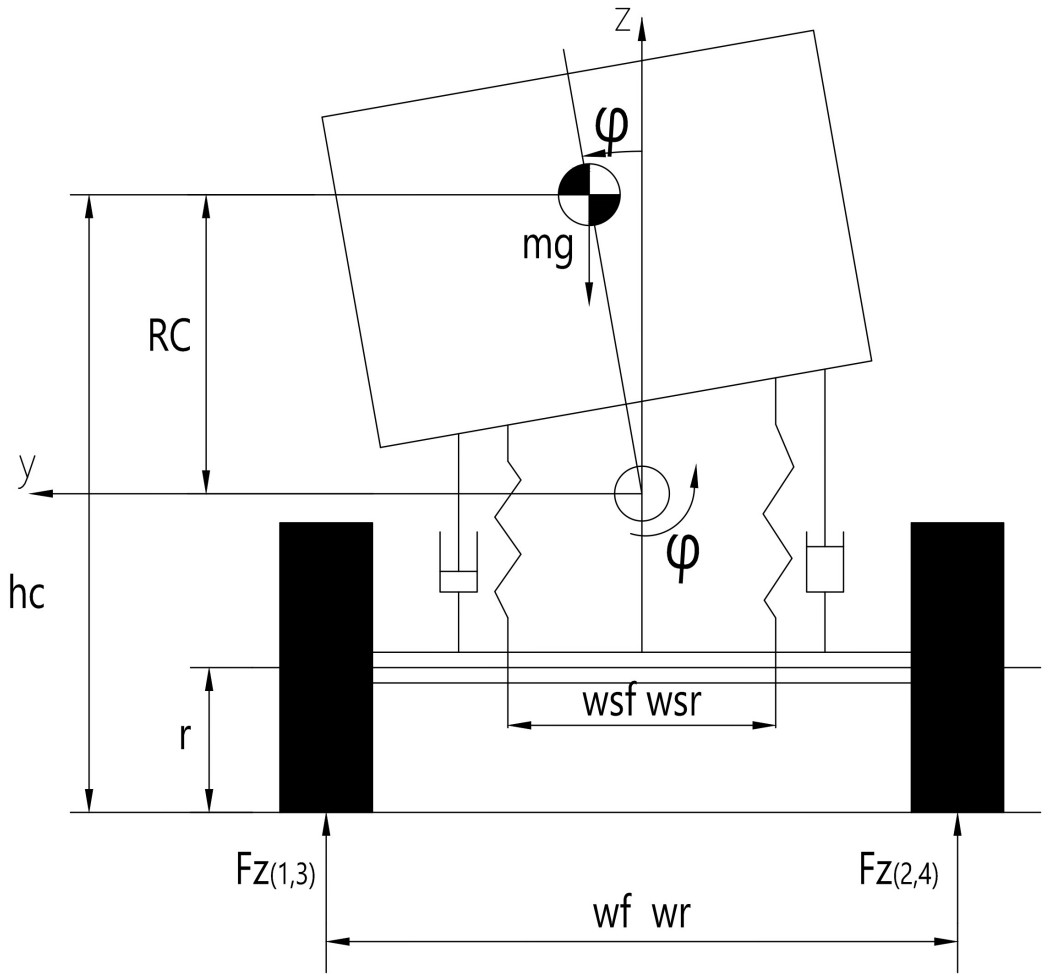

Figure 3.2: Two-track model front view

The corresponding vertical velocities are obtained as

$$\dot{z}_1 = \frac{w_{sf}\dot{\phi}}{\cos^2\phi} - \frac{l_f\dot{\theta}}{\cos^2\theta}, \tag{3.10}$$

$$\dot{z}_2 = -\frac{w_{sf}\dot{\phi}}{\cos^2\phi} - \frac{l_f\dot{\theta}}{\cos^2\theta}, \tag{3.11}$$

$$\dot{z}_3 = \frac{w_{sr}\dot{\phi}}{\cos^2\phi} + \frac{l_r\dot{\theta}}{\cos^2\theta}, \tag{3.12}$$

$$\dot{z}_4 = -\frac{w_{sr}\dot{\phi}}{\cos^2\phi} + \frac{l_r\dot{\theta}}{\cos^2\theta}. \tag{3.13}$$

The vertical suspension forces are computed from the baseline support force, the commanded force increment, and the equivalent vertical damping:

$$F_{z,1} = F_{z,1}^{\text{base}} + \Delta F_{z,FL} - \frac{1}{2}D_{z,f}\dot{z}_1, \tag{3.14}$$

$$F_{z,2} = F_{z,2}^{\text{base}} + \Delta F_{z,FR} - \frac{1}{2}D_{z,f}\dot{z}_2, \tag{3.15}$$

$$F_{z,3} = F_{z,3}^{\text{base}} + \Delta F_{z,RL} - \frac{1}{2}D_{z,r}\dot{z}_3, \tag{3.16}$$

$$F_{z,4} = F_{z,4}^{\text{base}} + \Delta F_{z,RR} - \frac{1}{2}D_{z,r}\dot{z}_4. \tag{3.17}$$

where $F_{z,i}^{\text{base}}$ is the baseline vertical support force, $\Delta F_{z,i}$ is the active force increment, and $D_{z,f}$ and $D_{z,r}$ are the equivalent front and rear vertical damping coefficients. The force-increment rates are constrained in the controller formulation, so the pneumatic actuator dynamics are kept outside the model formulation.

The vertical tire loads are then obtained as

$$F_{z,\text{tire},1} = \max\left(F_{z,\min},\ F_{z,1} + m_{u,f}g\right), \tag{3.18}$$

$$F_{z,\text{tire},2} = \max\left(F_{z,\min},\ F_{z,2} + m_{u,f}g\right), \tag{3.19}$$

$$F_{z,\text{tire},3} = \max\left(F_{z,\min},\ \frac{F_{z,3} + m_{u,r}g}{2}\right), \tag{3.20}$$

$$F_{z,\text{tire},4} = \max\left(F_{z,\min},\ \frac{F_{z,4} + m_{u,r}g}{2}\right). \tag{3.21}$$

The rear tire loads are halved to account for the dual-tire configuration. The lower bound $F_{z,\min}$ is a small numerical floor used by the nonlinear tire model. It prevents invalid tire-force calculations near zero normal load. Simulations involving actual wheel lift are outside the valid operating region of this model, and $F_{z,\min}$ is therefore chosen to remain small relative to the static tire load. These quantities provide the normal loads required by the nonlinear tire model and determine the suspension force distribution that contributes to the roll and pitch moments.

3.5 Lateral Dynamics

The lateral dynamics describe the tractor's motion along its body-fixed lateral axis. The response is governed by lateral tire forces, steering-force projection, and the

lateral hitch load. The equations follow the coupled rigid-body formulation used for optimization-oriented vehicle models [12].

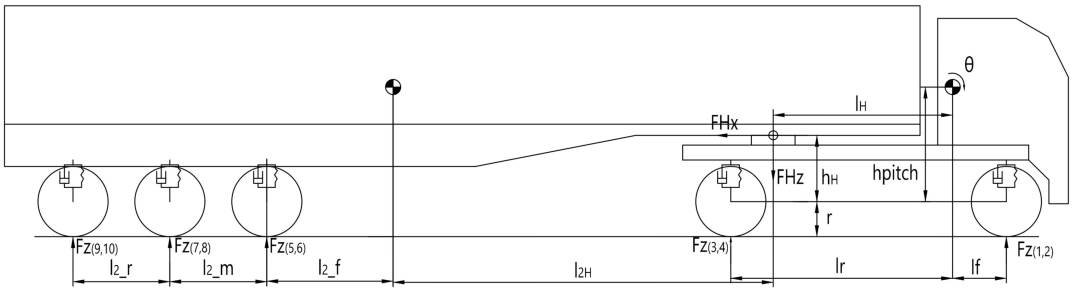

Figure 3.3: Two-track model side view

Figure 3.3 defines the longitudinal and vertical distances used in the pitch and hitch moment equations. The slip angles of the four wheels are written as

$$\alpha_1 = \tan^{-1}\left(\frac{v_y + l_f\dot{\psi}}{v_x}\right) - \delta_1, \tag{3.22}$$

$$\alpha_2 = \tan^{-1}\left(\frac{v_y + l_f\dot{\psi}}{v_x}\right) - \delta_2, \tag{3.23}$$

$$\alpha_3 = \tan^{-1}\left(\frac{v_y - l_r\dot{\psi}}{v_x}\right), \tag{3.24}$$

$$\alpha_4 = \tan^{-1}\left(\frac{v_y - l_r\dot{\psi}}{v_x}\right), \tag{3.25}$$

where α_i denotes the slip angle of wheel i, l_f and l_r are the longitudinal distances from the center of gravity to the front and rear axles, respectively, and δ_1 and δ_2 are the steering angles of the left and right front wheels.

The lateral tire force at each wheel is obtained from the nonlinear tire model,

$$F_{y,i} = \mathcal{F}_y(\alpha_i, F_{z,\text{tire},i}), \qquad i = 1, 2, 3, 4, \tag{3.26}$$

where $F_{z,\text{tire},i}$ is the corresponding vertical tire load.

The lateral force generated by the tractor is

$$\begin{aligned} F_{y,\text{veh}} = {} & (F_{x,1}\sin\delta_1 + F_{y,1}\cos\delta_1) + (F_{x,2}\sin\delta_2 + F_{y,2}\cos\delta_2) \\ & + F_{y,3} + F_{y,4}. \end{aligned} \tag{3.27}$$

Including the hitch-transmitted lateral force, the net lateral force acting on the tractor body becomes

$$F_y = F_{y,\text{veh}} - F_{Hy}. \tag{3.28}$$

The lateral acceleration can then be expressed as

$$\begin{aligned}\dot{v}_y = \frac{F_y}{m} - v_x\dot{\psi} + h_r\Big(&- \sin\theta\cos\phi\,\ddot{\psi} - \sin\phi\,\dot{\psi}^2 - 2\cos\theta\cos\phi\,\dot{\theta}\dot{\psi} \\ &+ \sin\theta\sin\phi\,\dot{\phi}\dot{\psi} - \sin\phi\,\dot{\phi}^2 + \cos\phi\,\ddot{\phi}\Big).\end{aligned} \tag{3.29}$$

In the yaw, roll, and pitch equations, F_x and F_y denote the net tractor-body forces resolved along the body-fixed longitudinal and lateral axes, respectively.

3.6 Yaw Dynamics

The yaw, roll, and pitch equations use the rigid-body rotational formulation described by Anistratov [12]. The yaw dynamics describe the rotation of the tractor body about its vertical axis. As shown in Figure 3.1, the axle distances, track widths, steering angles, and hitch position define the moment arms in the yaw equation. The total yaw moment is

$$\begin{aligned}M_Z = l_f\Big[&\left(F_{y,1}\cos\delta_1 + F_{x,1}\sin\delta_1\right) + \left(F_{y,2}\cos\delta_2 + F_{x,2}\sin\delta_2\right)\Big] \\ &- l_r\left(F_{y,3} + F_{y,4}\right) \\ &+ \frac{w_f}{2}\left(F_{y,1}\sin\delta_1 - F_{y,2}\sin\delta_2 - F_{x,1}\cos\delta_1 + F_{x,2}\cos\delta_2\right) \\ &+ \frac{w_r}{2}\left(-F_{x,3} + F_{x,4}\right) + F_{Hy}l_H.\end{aligned} \tag{3.30}$$

The yaw angular acceleration is then obtained as

$$\ddot{\psi} = \frac{M_Z - h_r\left(F_x\sin\phi + F_y\sin\theta\cos\phi\right)}{I_{xx}\sin^2\theta + \cos^2\theta\left(I_{yy}\sin^2\phi + I_{zz}\cos^2\phi\right)}. \tag{3.31}$$

As can be seen in Eq. (3.31), the yaw response is coupled to the roll and pitch states of the tractor body through both the effective inertia and the force-induced moment terms.

3.7 Roll Dynamics

The roll dynamics describe the rotational motion of the tractor body about its longitudinal axis. The roll response is mainly determined by the suspension force asymmetry, the equivalent roll stiffness and damping, the hitch-induced loads, and the nonlinear coupling with yaw and pitch motion.

As shown in Figure 3.2, the left-right suspension spacing and the vertical hitch geometry define the moment arms in the roll equation. The total roll moment acting on the tractor body is

$$\begin{aligned}M_X = w_{sf}\left(F_{z,1} - F_{z,2}\right) + w_{sr}\left(F_{z,3} - F_{z,4}\right) \\ - F_{Hy}\left(h_c - h_H\right) - T_{Hx},\end{aligned} \tag{3.32}$$

where $F_{z,i}$ denotes the vertical suspension force generated by suspension unit i, w_{sf} and w_{sr} are the half lateral spacings of the front and rear suspension units, F_{Hy} is the hitch-transmitted lateral force, and T_{Hx} is the hitch-induced roll moment.

The roll angular acceleration is given by

$$\begin{aligned}\ddot{\phi} = \frac{1}{I_{xx}\cos^2\theta + I_{yy}\sin^2\theta\sin^2\phi + I_{zz}\sin^2\theta\cos^2\phi}\Big[&M_X - K_{\phi,T}\phi - D_{\phi,T}\dot{\phi} \\ &+ h_r\left(F_y\cos\phi\cos\theta + mg\sin\phi\right) \\ &+ \dot{\psi}(I_{yy} - I_{zz})\left(\dot{\psi}\sin\phi\cos\phi\cos\theta + \dot{\phi}\sin\theta\sin\phi\cos\phi\right) \\ &+ \dot{\psi}\dot{\theta}\left(\cos^2\phi\, I_{yy} + \sin^2\phi\, I_{zz}\right)\Big].\end{aligned} \tag{3.33}$$

Since the active air suspension directly changes the vertical suspension forces, it also directly affects the roll moment acting on the tractor body.

3.8 Pitch Dynamics

The pitch dynamics describe the rotational motion of the tractor body about its lateral axis. The pitch response is affected by the front–rear distribution of suspension forces, the hitch-transmitted longitudinal and vertical loads, the gravitational restoring effect, and the nonlinear coupling among yaw, roll, and pitch motion.

As shown in Figure 3.3, the front and rear axle distances and the longitudinal and vertical hitch positions define the moment arms in the pitch equation. The total pitch moment acting on the tractor body is written as

$$\begin{aligned}M_Y = &-\left(F_{z,1} + F_{z,2}\right)l_f + \left(F_{z,3} + F_{z,4}\right)l_r \\ &- F_{Hz}l_H - F_{Hx}\left(h_c - h_H\right),\end{aligned} \tag{3.34}$$

where $F_{z,i}$ denotes the vertical suspension force generated by suspension unit i, l_f and l_r are the longitudinal distances from the center of gravity to the front and rear axles, respectively, F_{Hz} and F_{Hx} are the hitch-transmitted vertical and longitudinal forces, l_H is the longitudinal distance from the center of gravity to the hitch point, h_c is the center-of-gravity height, and h_H is the hitch height.

The pitch angular acceleration is then expressed as

$$\begin{aligned}\ddot{\theta} = \frac{1}{I_{yy}\cos^2\phi + I_{zz}\sin^2\phi}\Big[&M_Y - D_\theta\dot{\theta} \\ &+ h_{\text{pitch}}\left(mg\sin\theta\cos\phi - F_x\cos\theta\cos\phi\right) \\ &+ \dot{\psi}\Big(\dot{\psi}\sin\theta\cos\theta\left(I_{xx} - I_{yy} + \cos^2\phi\left(I_{yy} - I_{zz}\right)\right) \\ &\quad - \dot{\phi}\left(\cos^2\theta\, I_{xx} + \sin^2\phi\,\sin^2\theta\, I_{yy} + \sin^2\theta\,\cos^2\phi\, I_{zz}\right) \\ &\quad - \dot{\theta}\sin\theta\sin\phi\cos\phi\left(I_{yy} - I_{zz}\right)\Big)\Big].\end{aligned} \tag{3.35}$$

The denominator represents the effective pitch inertia, which depends on the instantaneous roll angle. The numerator includes the external pitch moment, the equivalent pitch damping, the contributions of gravity and longitudinal force, and the nonlinear rotational coupling terms. Through its effect on the suspension force distribution, the active air suspension influences the tractor's pitch response.

3.9 Validation Against the VTM Model

The control-oriented mathematical model is compared with the VTM Simscape plant model under the same input conditions. This comparison has a different purpose from the verification in Chapter 2. Chapter 2 checks whether the VTM suspension extension preserves the original passive response. The validation in this section checks whether the mathematical model captures the main motion needed by the controller.

3.9.1 Validation under Step Steering Input

In the first validation scenario, the vehicle initially travels in a straight line at a constant speed. A step steering input is then applied to both the mathematical and VTM models. The maneuver generates lateral acceleration and excites the tractor's roll dynamics. The steering input and the corresponding roll response comparison are shown in Figure 3.4.

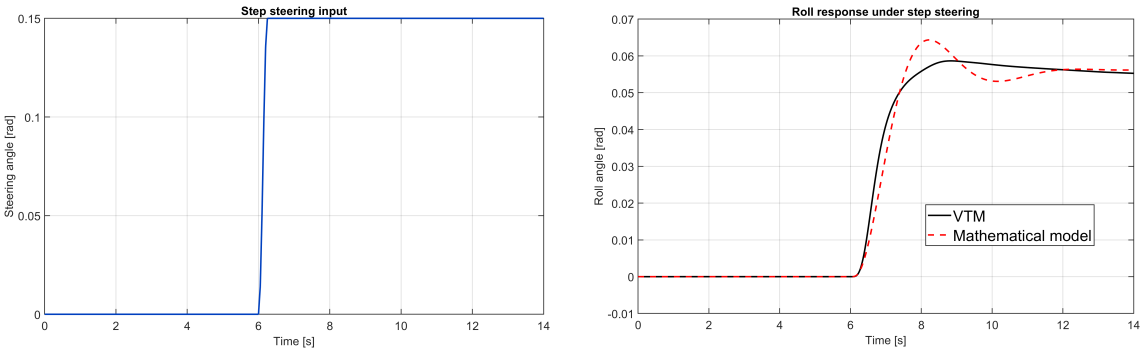

(a) Steering input (b) Roll response comparison

Figure 3.4: Step steering validation

The roll response of the mathematical model follows the main trend of the VTM response after the steering input is applied. The dominant roll build-up and the overall response level are captured in this representative case.

3.9.2 Validation under Straight-Line Braking

In the second validation scenario, the vehicle travels in a straight line, and a braking input is applied. Since no steering input is introduced, this case mainly excites the longitudinal and pitch dynamics. The longitudinal velocity and pitch response comparisons are shown in Figure 3.5.

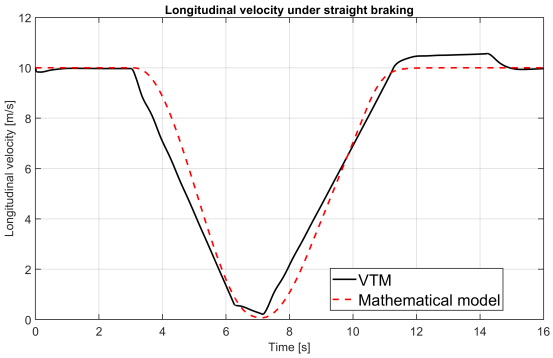

(a) Longitudinal velocity comparison

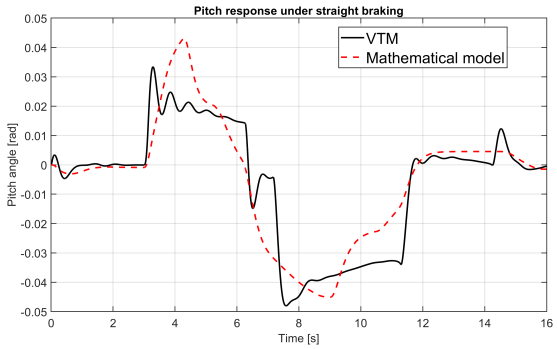

(b) Pitch response comparison

Figure 3.5: Straight braking validation

The mathematical model captures the main decrease in longitudinal velocity and the associated pitch motion in this representative braking case.

3.9.3 Summary of Validation Cases

To evaluate whether the mathematical model maintains an acceptable level of agreement with the high-fidelity VTM model under different operating conditions, additional steering and braking cases were performed. The step-steering amplitude was varied between 0.05, 0.10, and 0.15 rad at a constant vehicle speed of 10 m/s. The straight-line braking maneuver was evaluated at initial speeds of 8, 10, and 12 m/s. These cases extend the representative comparisons presented above and assess the model's consistency over a broader input range.

Before calculating the error metrics, the mean of each response prior to the input application was subtracted from the corresponding signal. This procedure only aligns the initial attitude reference and prevents small differences in the initial roll or pitch angle from influencing the comparison. No amplitude scaling, gain correction, or time shifting was applied. Consequently, the reported errors reflect the direct difference between the mathematical model and the VTM reference response.

Table 3.4 summarizes the root-mean-square error (RMSE) and maximum absolute error for the principal response variables. The corresponding time-domain plots are not repeated, as they exhibit trends similar to those of the representative cases shown previously. The validation matrix instead provides a concise overview of how the model discrepancy changes with steering amplitude and initial braking speed. The normalized value is calculated relative to the peak-to-peak range of the corresponding VTM reference signal:

$$\mathrm{NRMSE} = \frac{e_{\mathrm{RMSE}}}{\max(x_{\mathrm{VTM}}) - \min(x_{\mathrm{VTM}})} \times 100\%.$$

Test group	Input	Response	RMSE	Maximum error	NRMSE [%]
Step steering	0.05 rad	Roll [deg]	0.0989	0.2390	5.67
Step steering	0.10 rad	Roll [deg]	0.1131	0.4343	4.99
Step steering	0.15 rad	Roll [deg]	0.1574	0.5539	4.69
Straight braking	8 m/s	v_x [m/s]	0.1996	0.3784	1.958
Straight braking	8 m/s	Pitch [deg]	0.0594	0.1385	1.056
Straight braking	10 m/s	v_x [m/s]	0.0594	0.1785	0.573
Straight braking	10 m/s	Pitch [deg]	0.0529	0.1579	1.132
Straight braking	12 m/s	v_x [m/s]	0.1833	0.2499	1.764
Straight braking	12 m/s	Pitch [deg]	0.0499	0.1675	1.068

Table 3.4: Error metrics for the mathematical-model validation cases.

For the steering cases, both the RMSE and the maximum roll error increase with increasing steering amplitude. This indicates that the difference between the control-oriented mathematical model and the VTM model becomes more pronounced under stronger lateral excitation. Nevertheless, the mathematical model preserves the direction, overall shape, and dominant dynamics of the roll response throughout the tested input range.

The braking results show that the model retains the main longitudinal speed and pitch characteristics across all three initial speeds. The pitch RMSE remains within a narrow range of approximately 0.05–0.06 deg, with no systematic deterioration as the initial speed increases. The longitudinal-speed error varies between the tested cases but remains sufficiently small to represent the dominant deceleration behavior required by the prediction model.

The remaining discrepancies are expected because the mathematical model is intentionally simplified and does not include all high-frequency dynamics and subsystem details represented in the VTM environment. Its purpose is therefore not to reproduce every local or transient feature of the high-fidelity model, but to capture the dominant vehicle dynamics relevant to controller prediction and optimization.

Overall, the repeated validation cases demonstrate that the mathematical model provides a consistent representation of the roll, pitch, and longitudinal-speed responses over the tested operating range. The level of agreement achieved is considered sufficient for use in model-based control design.

4

Controller Design

The controller is based on the NMPC and air-suspension framework developed in [10]. The controller in [10] did not include the semitrailer configuration studied here. It also used fixed mass-flow-related quantities in the prediction model. In the present work, the vehicle prediction and pneumatic actuation are separated. Pitch states, hitch coupling, and a bounded coupling-preview term are added. Pneumatic authority is represented through force, force-rate, pressure, and mass-flow related limits.

4.1 Control Objectives

The main objective of the controller is to improve vehicle attitude stability during cornering maneuvers by actively redistributing the vertical suspension forces, i.e., roll dynamics. As excessive roll angle, roll rate, and lateral load transfer are directly related to rollover risk in heavy-duty vehicle combinations.

Pitch motion is treated as the second attitude-control objective. It is included in the NMPC state and in the cost function. Pitch angle and pitch rate have their own weights. These terms limit unwanted front-to-rear motion during suspension force redistribution, especially during braking. Their weights remain lower than the roll weights because rollover safety is the main objective.

The controller should also avoid unnecessarily aggressive changes in force and pressure. The resulting commands must remain compatible with the limited response speed and pressure range of the pneumatic actuation system. Overall, the control problem is formulated as a constrained predictive attitude-control problem, with roll stability as the primary target and pitch regularization, actuator smoothness, and physical limitations as supporting considerations.

4.2 Control Architecture

The proposed active suspension controller is organized as a layered closed-loop structure, as shown in Fig. 4.1. Sensors provide measured vehicle states, steering input, hitch signals, and air spring pressures; in the thesis, these are generated by the VTM model. Based on these signals, the upper-layer NMPC predicts the future vehicle response and computes the desired four-corner vertical force increments.

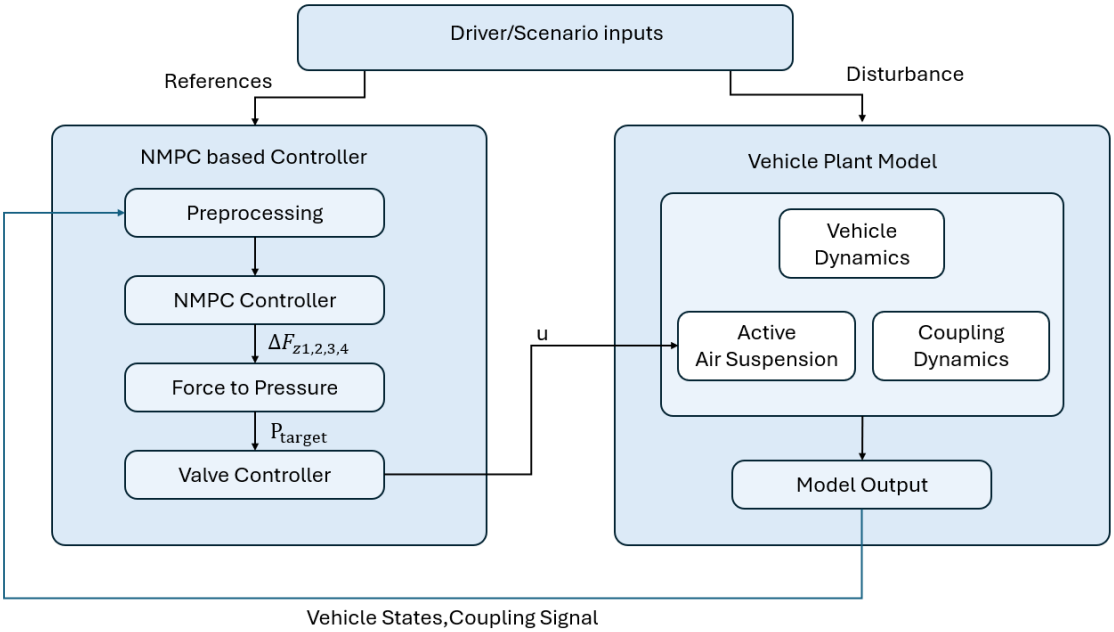

Figure 4.1: Active suspension controller structure.

The force increments are passed to a force-to-pressure allocation layer that converts the requested vertical force changes into air-spring pressure references. These pressure references are tracked by the lower-level pressure controller and valve logic, which command filling, holding, or venting of each air spring. The resulting pressure changes modify the suspension forces in the VTM plant, and the updated states and pressures are fed back to close the loop.

The proposed architecture separates the high-level attitude-control problem from the pneumatic actuation problem. The NMPC decides how the suspension forces should be redistributed, while the lower layers handle pressure conversion, pressure tracking, and valve implementation.

The main layer interfaces are summarized in Table 4.1. The table focuses on the signals that connect the controller layers, rather than listing every implementation variable.

Signal	Used by	Main role
x	NMPC	Reduced vehicle attitude and motion state
δ_k	NMPC	Steering input over the prediction horizon
F_H, T_H	NMPC	Hitch force and moment disturbances
P_{meas}	NMPC/allocation	Pressure feedback for current force and rate limits
ν	NMPC decision	Force-increment rate
$\Delta F_z^\star$	NMPC output	Desired four-corner force increment
$P^\star$	Allocation output	Air spring pressure reference
u_v	Valve logic	Fill, hold, or vent command

Table 4.1: Controller layer interfaces

4.3 Controller Variables and Layer Interfaces

The upper-layer controller uses a reduced-order vehicle state vector rather than the full state vector of the VTM plant. The vehicle states used are

$$x = \begin{bmatrix} v_x & v_y & \psi & \dot{\psi} & \phi & \dot{\phi} & \theta & \dot{\theta} \end{bmatrix}^T, \tag{4.1}$$

where v_x and v_y are the longitudinal and lateral velocities, ψ and $\dot{\psi}$ are the yaw angle and yaw rate, ϕ and $\dot{\phi}$ are the roll angle and roll rate, and θ and $\dot{\theta}$ are the pitch angle and pitch rate.

The upper layer does not directly control valve states. Its main output is the desired four-corner vertical suspension force increments,

$$\Delta F_z^\star = \begin{bmatrix} \Delta F_{z,\text{FL}}^\star & \Delta F_{z,\text{FR}}^\star & \Delta F_{z,\text{RL}}^\star & \Delta F_{z,\text{RR}}^\star \end{bmatrix}^T. \tag{4.2}$$

These increments represent the additional support force requested from the active air suspension relative to the baseline suspension force at each corner.

Since the pneumatic actuator cannot change the generated force instantaneously, the force increment is included as an augmented NMPC state,

$$z_k = \begin{bmatrix} x_k \\ \Delta F_{z,k} \end{bmatrix}. \tag{4.3}$$

The NMPC input is selected as the force-increment rate,

$$\nu_k = \Delta \dot{F}_{z,k} = \begin{bmatrix} \Delta \dot{F}_{z,\text{FL},k} & \Delta \dot{F}_{z,\text{FR},k} & \Delta \dot{F}_{z,\text{RL},k} & \Delta \dot{F}_{z,\text{RR},k} \end{bmatrix}^T. \tag{4.4}$$

The force increment is propagated over one controller sampling interval as

$$\Delta F_{z,k+1} = \Delta F_{z,k} + T_s \nu_k, \tag{4.5}$$

where T_s is the sampling time. This formulation allows constraining both the magnitude of the force and the rate at which it is built up or released.

4.4 Trailer Preview Treatment

In this section, preview refers to a bounded correction added to the measured hitch roll moment using the upcoming steering input over the prediction horizon. The correction is not intended to replace a full trailer model or to predict the complete trailer state. It is used only to reduce the underestimation of the early trailer-induced roll disturbance before this disturbance is fully visible in the measured hitch signal. The trailer influence is included through the measured hitch forces and moments. Instead of introducing the hitch signal as an indexed vector, the physically relevant quantities are expressed as the longitudinal, lateral, and vertical hitch reactions, as well as the hitch roll moment. The longitudinal and lateral reactions are first measured in the hitch frame γ and then transformed into the tractor body frame $\mathcal{B}$ using the current hitch angle ψ_H:

$$F_{Hx} = F'_{Hx}\cos(\gamma) + F'_{Hy}\sin(\gamma), \tag{4.6}$$

$$F_{Hy} = F'_{Hy}\cos(\gamma) - F'_{Hx}\sin(\gamma). \tag{4.7}$$

The vertical hitch force and hitch roll moment are denoted by

$$F_{Hz} = F'_{Hz}, \qquad T_{Hx} = T'_{Hx}. \tag{4.8}$$

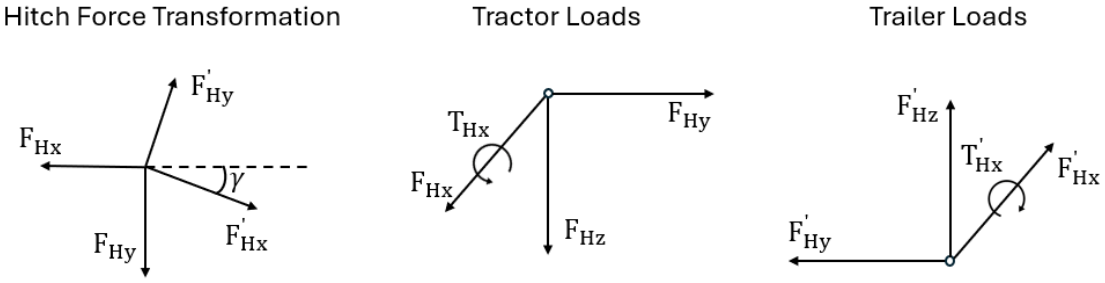

Figure 4.2: Hitch Force and Moment Transformation

These hitch terms are treated as external disturbances in the tractor prediction model. In particular, the lateral hitch force and hitch roll moment directly affect the predicted roll dynamics. The roll moment contribution is written as

$$M_x = M_{x,\text{susp}} - F_{Hy}(h_c - h_H) - T_{Hx}, \tag{4.9}$$

where h_c is the tractor center-of-gravity height and h_H is the hitch height.

Over the prediction horizon, the measured hitch forces are held constant, while the hitch roll moment is allowed to include a bounded preview correction. This correction represents the early trailer-induced roll disturbance associated with the upcoming steering input:

$$\Delta T_{Hx,k} = s_H c_H m_t h_t \frac{v_x^2}{L_{\text{eff}}}(\bar{\delta}_k - \bar{\delta}_0), \tag{4.10}$$

where m_t is the trailer mass, h_t is the effective trailer roll moment height, L_{eff} is an effective curvature length, c_H is the hitch-coupling factor, s_H sets the sign convention, and $\bar{\delta}_k$ is the representative steering angle at prediction step k. Only a fraction of this trailer-induced roll moment is transmitted to the tractor through the hitch, which is represented by the coupling factor c_H. The predicted hitch roll moment is then

$$\hat{T}_{Hx,k} = T_{Hx,0} + \text{sat}\left(\Delta T_{Hx,k},\ -T_{Hx,\max},\ T_{Hx,\max}\right). \tag{4.11}$$

The preview correction follows a quasi-static approximation. For small steering angles,

$$\kappa \approx \frac{\delta}{L_{\text{eff}}}, \tag{4.12}$$

and therefore

$$a_y \approx \frac{v_x^2}{L_{\text{eff}}}\delta. \tag{4.13}$$

The trailer lateral inertial force and roll moment are approximated as

$$F_{y,t} \approx m_t a_y, \qquad M_{\text{roll},t} \approx m_t a_y h_t. \tag{4.14}$$

4.5 Upper-layer NMPC Controller

The upper layer is formulated as a nonlinear model predictive controller. Its role is to compute a feasible four-corner suspension force redistribution based on the measured vehicle state, steering preview, hitch disturbance, and air spring pressures. The vehicle dynamics used by the controller follow the nonlinear tractor model introduced in the modeling chapter; this section focuses on how the model is implemented within the controller.

4.5.1 Prediction Model

The NMPC uses a discrete-time nonlinear model of the form

$$x_{k+1} = f_d(x_k, \Delta F_{z,k}, \delta_k, \hat{H}_k), \tag{4.15}$$

where x_k is the predicted vehicle state, $\Delta F_{z,k}$ is the four-corner force increment, δ_k is the steering input, and $\hat{H}_k$ denotes the transformed hitch disturbances including the bounded roll-moment correction. The continuous-time two-track tractor model introduced in Chapter 3 is discretized over the controller sampling interval.

Using the augmented state in Eq. (4.3), the augmented discrete-time model is

$$z_{k+1} = \begin{bmatrix} f_d(x_k, \Delta F_{z,k}, \delta_k, \hat{H}_k) \\ \Delta F_{z,k} + T_s \nu_k \end{bmatrix}. \tag{4.16}$$

The initial condition is set from the measured vehicle state and the current force increment inferred from the measured air spring pressures. The pressure measurements are also used to estimate feasible force-rate bounds, so that the optimized force-rate command remains consistent with the available pneumatic authority.

4.5.2 Numerical Settings

The controller model uses the same sampling time, $T_s = 0.05$ s. The prediction horizon is $N_p = 100$, giving a total prediction horizon of 5.0 s. A force-rate decision is defined at every time step, so the control horizon is also 100 steps. The NMPC optimization and control commands are updated every second model sample. The control-update interval is therefore 0.10 s, and the first optimized command is held during the intermediate 0.05 s sample.

Setting	Symbol	Value
Controller sample time	T_s	0.05 s
Prediction-model sample time	T_s	0.05 s
Prediction horizon	N_p	100 steps
Control horizon	N_u	100 steps
Prediction time	$N_p T_s$	5.0 s
Control update time	T_{update}	0.10 s
Dynamic-rate safety factor	η_r	0.90
IPOPT tolerance		5×10^{-4}
IPOPT acceptable tolerance		3×10^{-3}
IPOPT maximum iterations		70

Table 4.2: NMPC numerical settings

4.5.3 Cost Function

The finite-horizon objective function is

$$\begin{aligned} J = \sum_{k=0}^{N_p-1} \Big[& (x_k - x_{\text{ref},k})^T Q_x (x_k - x_{\text{ref},k}) + (\Delta F_{z,k} - \Delta F_{z,\text{ref},k})^T Q_F (\Delta F_{z,k} - \Delta F_{z,\text{ref},k}) \\ & + \nu_k^T R_\nu \nu_k + \Delta \nu_k^T S_\nu \Delta \nu_k \Big] \\ & + (x_{N_p} - x_{\text{ref},N_p})^T Q_N (x_{N_p} - x_{\text{ref},N_p}). \end{aligned} \tag{4.17}$$

The input variation is defined as

$$\Delta \nu_k = \nu_k - \nu_{k-1}. \tag{4.18}$$

The state-weighting matrix is structured as

$$Q_x = \text{diag}\left(q_{v_x},\, q_{v_y},\, q_\psi,\, q_{\dot\psi},\, q_\phi,\, q_{\dot\phi},\, q_\theta,\, q_{\dot\theta}\right). \tag{4.19}$$

The numerical weights were tuned manually based on repeated simulation tests. Different weight combinations were tested under steering and combined steering-and-braking conditions. The roll weights were adjusted first to reduce the roll response and LTR. The pitch weights were then tuned based on the braking response. Finally, the penalties on force and force rate were adjusted to avoid excessive actuator effort

and abrupt changes in the control commands. The same final weighting matrices were used for all NMPC results.

The values used in the simulations are

$$Q_x = \mathrm{diag}\left(0,\ 0,\ 0,\ 0,\ 7.5 \times 10^4,\ 4.0 \times 10^2,\ 1.5 \times 10^4,\ 1.2 \times 10^2\right), \tag{4.20}$$

$$Q_N = Q_x, \tag{4.21}$$

$$Q_F = \mathrm{diag}\left(1.0 \times 10^{-6},\ 1.0 \times 10^{-6},\ 1.2 \times 10^{-6},\ 1.2 \times 10^{-6}\right), \tag{4.22}$$

$$R_\nu = 2.0 \times 10^{-8} I_4, \tag{4.23}$$

$$S_\nu = 8.0 \times 10^{-8} I_4. \tag{4.24}$$

The four entries of Q_F correspond to the front-left, front-right, rear-left, and rear-right force increments. The largest state weights are assigned to roll angle and roll rate. Pitch angle and pitch rate are included as secondary attitude-control terms, with smaller weights than the roll states. At each control update, $x_{\mathrm{ref},k}$ is initialized from the measured state. The roll-rate, pitch-angle, and pitch-rate references are set to zero, while the bounded roll-angle reference is generated from the steering preview. The force reference $\Delta F_{z,\mathrm{ref},k}$ is generated from a bounded roll-moment request distributed between the front and rear suspension lever arms; a front–rear component is added when braking activates the pitch-control channel. The force reference $\Delta F_{z,\mathrm{ref},k}$ represents the desired force redistribution used to support the attitude objective, while R_ν and S_ν limit the magnitude and variation of the force-rate command.

Weight	Penalized term	Main purpose
Q_x	Vehicle-state error	Roll-dominant and pitch-aware attitude control
Q_N	Terminal state error	End-of-horizon attitude penalty
Q_F	Force-reference error	Shape the desired force redistribution
R_ν	Force-increment rate	Limit actuator effort
S_ν	Force-rate variation	Improve command smoothness

Table 4.3: NMPC weighting terms

4.5.4 Constraints

The optimization problem is subject to the prediction model, force-amplitude limits, fixed absolute force-rate limits, and pressure-dependent dynamic force-rate limits:

$$\begin{aligned}
\min_{z_k,\nu_k} \quad & J \\
\text{s.t.} \quad & z_0 = z_{\text{meas}}, \\
& z_{k+1} = \begin{bmatrix} f_d(x_k, \Delta F_{z,k}, \delta_k, \hat{H}_k) \\ \Delta F_{z,k} + T_s \nu_k \end{bmatrix}, \\
& \Delta F_{z,\min} \le \Delta F_{z,k} \le \Delta F_{z,\max}, \\
& \nu_{\min}^{\text{abs}} \le \nu_k \le \nu_{\max}^{\text{abs}}, \\
& \nu_{\min,k}^{\text{dyn}} \le \nu_k \le \nu_{\max,k}^{\text{dyn}}, \\
& k = 0, \dots, N_p - 1.
\end{aligned} \tag{4.25}$$

The fixed bounds $\nu_{\min}^{\text{abs}}$ and $\nu_{\max}^{\text{abs}}$ impose the maximum allowed force-increment rate. Additional limits are calculated at each operating point using the current air-spring pressure, chamber volume, and valve mass-flow capacity. For the air-spring corner i, the chamber volume used by the rate estimate is

$$V_{i,k} = \max\left(V_{0,i} + A_{\text{eff},i} z_{i,k},\ V_{\min}\right), \tag{4.26}$$

where $z_{i,k}$ is the predicted suspension deflection at that corner. Using the measured pressure $P_{\text{meas},i,k}$, the fill and vent force-rate limits are estimated as

$$\dot{F}_{i,k}^{\text{fill}} = A_{\text{eff},i} \frac{RT}{V_{i,k}} \dot{m}_{\text{in,max}}(P_{\text{meas},i,k}), \tag{4.27}$$

$$\dot{F}_{i,k}^{\text{vent}} = A_{\text{eff},i} \frac{RT}{V_{i,k}} \dot{m}_{\text{out,min}}(P_{\text{meas},i,k}), \tag{4.28}$$

where $\dot{m}_{\text{in,max}}$ and $\dot{m}_{\text{out,min}}$ are obtained from the valve flow model. For the four-corner controller, these cornerwise rates define the dynamic NMPC input bounds as

$$\nu_{\min,k}^{\text{dyn}} = \eta_r \begin{bmatrix} \dot{F}_{\text{FL},k}^{\text{vent}} \\ \dot{F}_{\text{FR},k}^{\text{vent}} \\ \dot{F}_{\text{RL},k}^{\text{vent}} \\ \dot{F}_{\text{RR},k}^{\text{vent}} \end{bmatrix}, \tag{4.29}$$

$$\nu_{\max,k}^{\text{dyn}} = \eta_r \begin{bmatrix} \dot{F}_{\text{FL},k}^{\text{fill}} \\ \dot{F}_{\text{FR},k}^{\text{fill}} \\ \dot{F}_{\text{RL},k}^{\text{fill}} \\ \dot{F}_{\text{RR},k}^{\text{fill}} \end{bmatrix}. \tag{4.30}$$

where the implemented safety margin is $\eta_r = 0.90$. If a modal front–rear force representation is used, the same cornerwise fill, and vent rates are combined, for example,

$$\dot{\Delta F}_{z,f,\min}^{\text{dyn}} = \eta_r \left(\dot{F}_{\text{FL}}^{\text{vent}} - \dot{F}_{\text{FR}}^{\text{fill}}\right), \qquad \dot{\Delta F}_{z,f,\max}^{\text{dyn}} = \eta_r \left(\dot{F}_{\text{FL}}^{\text{fill}} - \dot{F}_{\text{FR}}^{\text{vent}}\right), \tag{4.31}$$

$$\dot{\Delta F}_{z,r,\min}^{\text{dyn}} = \eta_r \left(\dot{F}_{\text{RL}}^{\text{vent}} - \dot{F}_{\text{RR}}^{\text{fill}}\right), \qquad \dot{\Delta F}_{z,r,\max}^{\text{dyn}} = \eta_r \left(\dot{F}_{\text{RL}}^{\text{fill}} - \dot{F}_{\text{RR}}^{\text{vent}}\right). \tag{4.32}$$

Thus, the optimizer is not only limited by prescribed force and rate bounds; it is also restricted by the instantaneous pneumatic authority available at the measured pressure operating point. Pressure saturation is not imposed directly as an NMPC state constraint; instead, it is handled by the allocation and lower-level pressure-control layers.

The controller is implemented in MATLAB/Simulink using CasADi and IPOPT. The nonlinear prediction model is integrated by fourth-order Runge–Kutta with three substeps in each 0.05 s prediction interval. The previous optimal state and input sequences are shifted by one step and used as the next initial guess.

4.6 Force-to-Pressure Allocation

The NMPC output is a desired four-corner vertical suspension force increment $\Delta F_z^\star$. Since the physical actuator is an air spring, this force demand is converted into pressure references. The air spring force is approximated by

$$F_{z,i} = (P_i - P_{\text{atm}})A_{\text{eff},i}, \tag{4.33}$$

where P_i is the absolute pressure, P_{atm} is the atmospheric pressure, and $A_{\text{eff},i}$ is the effective air spring area at corner i.

Using this relation, the desired pressure reference at each air spring is computed from the baseline pressure and the desired force increment:

$$P_i^\star = P_{\text{base},i} + \frac{\Delta F_{z,i}^\star}{A_{\text{eff},i}}. \tag{4.34}$$

The pressure reference is limited by the admissible pressure range:

$$P_{\min} \le P_i^\star \le P_{\max}. \tag{4.35}$$

The force-to-pressure allocation layer maps each requested force increment $\Delta F_{z,i}^\star$ to the corresponding pressure reference $P_i^\star$. This pressure reference is then passed to the pressure-tracking and valve-logic layer.

4.7 Pressure Tracking and Valve Logic

The lower layer receives the pressure reference $P_i^\star$ computed by the force-to-pressure allocation layer defined in Section 4.6. For each air spring, the pressure error is

$$e_{P,i} = P_i^\star - P_{\text{meas},i}. \tag{4.36}$$

Both the pressure reference and measured pressure are limited to the implemented range of 1.0 to 12 bar before the error is calculated. The controller regulates the pressure using three operating states. Its valve state is

$$q_i \in \{-1, 0, 1\}, \qquad q_i = \begin{cases} 1, & \text{fill}, \\ 0, & \text{hold}, \\ -1, & \text{vent}. \end{cases} \tag{4.37}$$

When the valve is closed, it opens for filling if $e_{P,i} > e_{\text{on},i}$ and opens for venting if $e_{P,i} < -e_{\text{on},i}$. During filling, it closes when $e_{P,i} < e_{\text{off},i}$. During venting, it closes when $e_{P,i} > -e_{\text{off},i}$. A large error with the opposite sign can switch the valve directly from filling to venting or from venting to filling.

Tractor axle	e_{on} [bar]	e_{off} [bar]
Front air springs	0.08	0.02
Rear air springs	0.10	0.03

Table 4.4: Pressure controller thresholds

The thresholds $e_{\text{on},i}$ and $e_{\text{off},i}$ listed in Table 4.4 prevent rapid switching near the pressure reference. The valve command sent to the air-spring model is $u_{v,i} = q_i$.

4.8 Baseline Controllers

Two baseline cases are used for comparison. The first is the passive baseline. It retains the original vertical springs and dampers in the VTM rather than replacing them with actively controlled air-spring forces.

The second baseline is the height-based PID controller inherited from [10]. It uses the same air-suspension pressure and valve interface as the proposed controller, but it does not use predictive control, steering preview, or hitch preview. For each controlled suspension height h_i, the height signal is first offset by its initial value. The reference is then zero,

$$e_{h,i}(t) = h_i(0) - h_i(t). \tag{4.38}$$

The PID request has the standard form

$$u_{\text{PID},i} = K_{p,i} e_{h,i} + K_{i,i} \int e_{h,i}\, dt + K_{d,i} \dot{e}_{h,i}. \tag{4.39}$$

The gains are inherited from the four-corner height controller in the previous thesis [10] and were not retuned here. The same settings are used at all four corners. This baseline keeps each controlled height close to its initial value. It does not optimize roll, pitch, or trailer response.

5

Simulation Setup and Evaluation Metrics

5.1 Vehicle and Controller Cases

The simulation plant is a 4x2 tractor connected to a three-axle semitrailer. Active air suspension is installed only on the tractor. The semitrailer keeps its passive suspension in every test.

Three controller cases are compared. The passive baseline retains the original vertical springs and dampers. The PID case replaces the tractor suspension with the air-suspension model and controls each suspension height relative to its initial value. The NMPC case uses the same air-suspension plant but calculates four force increments based on the predicted roll, pitch, steering, and hitch responses.

The vehicle configuration, payload, road, initial condition, steering command, and braking command are the same for all three cases. The steering and braking commands are open-loop inputs. No target path or path-tracking controller is used. The trajectory plots, therefore, compare vehicle response under the same driver input. They do not measure path-tracking error.

5.2 Test Maneuvers

The closed-loop controller comparison uses the six maneuver cases listed in Table 5.1. Step steering gives a rapid lateral excitation. Ramp steering gives a smoother build-up. The standard lane change includes a faster steering reversal. The slow lane change applies its steering action over 8 s. Straight braking is used for pitch and braking-distance checks. Steering while braking excites both roll and pitch simultaneously.

The steering-only and steering-braking cases use an initial speed of 10 m/s and a maximum steering input of 0.15 rad, which is approximately 8.59°. The step and ramp inputs begin at $t = 6$ s. The steering-braking case uses the model's curved steering input and an open-loop brake command until the vehicle stops.

Case	Initial speed	Steering input	Braking input
Step steering	10 m/s	Step to 0.15 rad	None
Ramp steering	10 m/s	Ramp to 0.15 rad	None
Lane change	10 m/s	Reversing input	None
Slow lane change	10 m/s	0.10 rad over 8 s	None
Straight braking	10 m/s	None	Open-loop braking
Steering-braking	10 m/s	Curved input	Open-loop braking

Table 5.1: Current closed-loop comparison cases.

The slow lane-change steering starts at $t = 4$ s and ends at $t = 12$ s. It is evaluated separately because its longer time scale gives the pneumatic suspension more time to respond.

5.3 Evaluation Metrics

The load transfer ratio (LTR) is the primary rollover metric. Trailer LTR is calculated from the vertical tire loads on the three trailer axles:

$$\mathrm{LTR}_{\mathrm{trailer}} = \frac{(F_{z,L3} + F_{z,L4} + F_{z,L5}) - (F_{z,R3} + F_{z,R4} + F_{z,R5})}{(F_{z,L3} + F_{z,L4} + F_{z,L5}) + (F_{z,R3} + F_{z,R4} + F_{z,R5})} \tag{5.1}$$

and is a value between -1 and 1. A value near zero means that the left and right loads are close. Values near either limit, ± 1, mean that one side carries very little vertical load, and a rollover is imminent. The warning threshold is set as $|\mathrm{LTR}| = 0.8$. Tractor LTR is calculated in the same way from the two tractor axles. Roll angle is used as a supporting measure of lateral body motion. Pitch angle is used in braking cases to assess the front-rear attitude response.

Lateral acceleration is also used to assess whether the suspension controller affects lateral motion. The understeer-gradient relation is

$$\delta \approx \frac{L}{R} + K_{\mathrm{u}} a_y, \tag{5.2}$$

where K_{u} is the understeer gradient [1]. This relation describes the steering balance of the tractor or an equivalent single unit. It does not, by itself, show whether lateral acceleration is amplified from the tractor to the semitrailer. Therefore, trailer lateral acceleration and rearward amplification are included as additional lateral-response metrics. Rearward amplification is defined as the peak trailer lateral acceleration divided by the peak tractor lateral acceleration,

$$RA = \frac{\max |a_{y,\mathrm{trailer}}|}{\max |a_{y,\mathrm{tractor}}|}. \tag{5.3}$$

For both braking cases, braking distance starts at the first brake command, and it ends when the longitudinal speed reaches

$$v_x \leq 0.05 \text{ m/s}. \tag{5.4}$$

Distance traveled before brake application is excluded. The distance is calculated from the cumulative x-y path between these two times. This also covers the curved steering-braking case.

6

Results and Analysis

The simulation settings, controller variants, and evaluation metrics are defined in Chapter 5. This chapter uses those definitions to compare the passive baseline, PID controller, and NMPC controller. The discussion first focuses on the primary rollover-safety objective, namely roll and load transfer. It then expands the analysis to the stability boundary, handling response, trajectory, and stopping distance.

6.1 Roll and Load Transfer Response

The core objective of the active suspension controller is rollover prevention. Therefore, this section first examines LTR and roll angle in the time domain. The trailer is the most critical unit in severe steering cases, while the active suspension is installed only on the tractor. This makes the trailer response a direct test of whether the controller can use tractor-side actuation to improve the passive semitrailer's rollover margin.

6.1.1 Step Steering Transient Response

The step-steering case uses an initial speed of 10 m/s and a maximum steering input of 0.15 rad. The steering command starts at $t = 6$ s and produces the most abrupt lateral excitation among the steering-only maneuvers. This case is therefore used as the main transient test for the rollover controller.

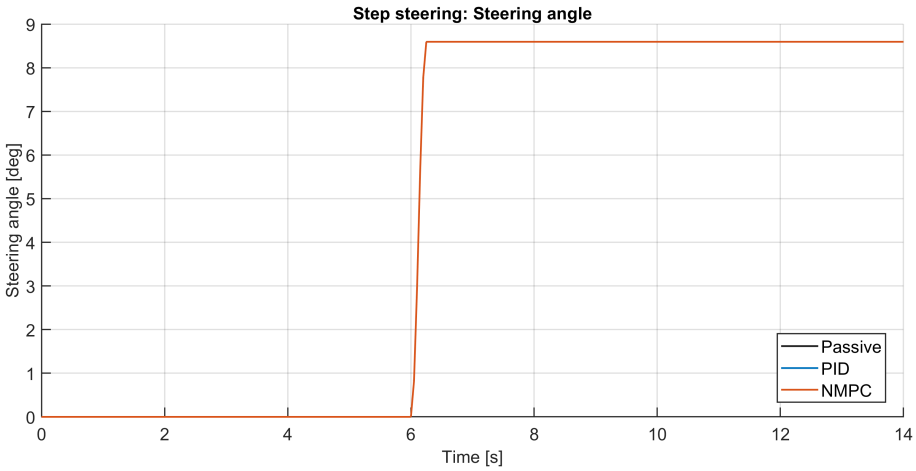

Figure 6.1: Step steering input

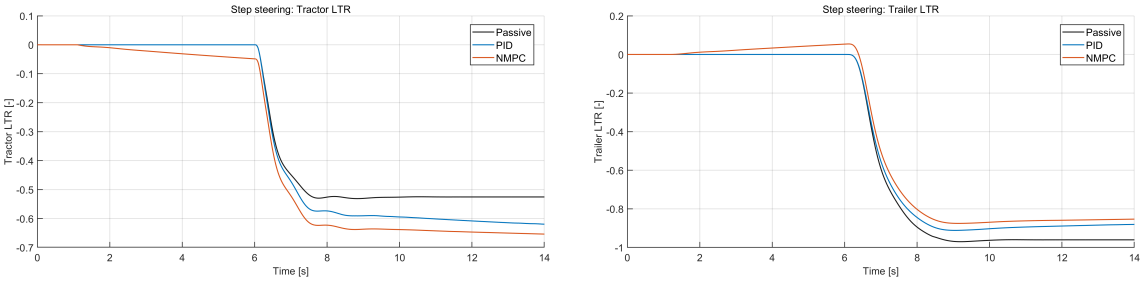

(a) Tractor LTR (b) Trailer LTR

Figure 6.2: LTR response under step steering

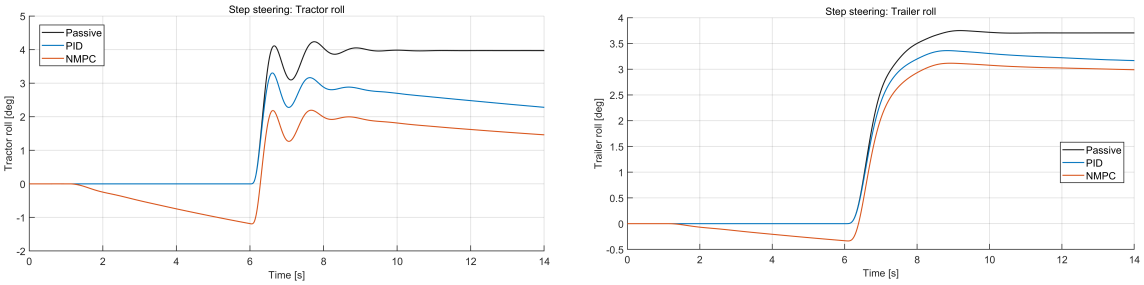

(a) Tractor roll (b) Trailer roll

Figure 6.3: Roll response under step steering

In the step-steering case, the peak trailer LTR decreases from 0.970 with the passive suspension to 0.912 with PID and 0.875 with NMPC. The peak trailer roll angle decreases from 3.75° to 3.12° with NMPC. These changes correspond to reductions of 9.8% in trailer LTR and 16.9% in trailer roll angle relative to the passive baseline. In this test, the NMPC builds corrective suspension force during the abrupt lateral excitation.

The tractor LTR follows the opposite trend: it increases from 0.531 with the passive suspension to 0.654 with NMPC. This is not a failure of the controller. Since the active suspension is only installed on the tractor, the tractor must generate a left–right vertical force difference to influence the passive trailer through the fifth wheel. The NMPC therefore uses part of the available tractor load-transfer margin to reduce the more critical trailer LTR.

6.1.2 Ramp Steering Response

The ramp-steering case uses the same initial speed and maximum steering angle as the step case, namely 10 m/s and 0.15 rad. The difference is that the steering input rises more gradually. This reduces the abruptness of the lateral excitation and is useful for checking whether the controller benefit remains when the maneuver is smoother.

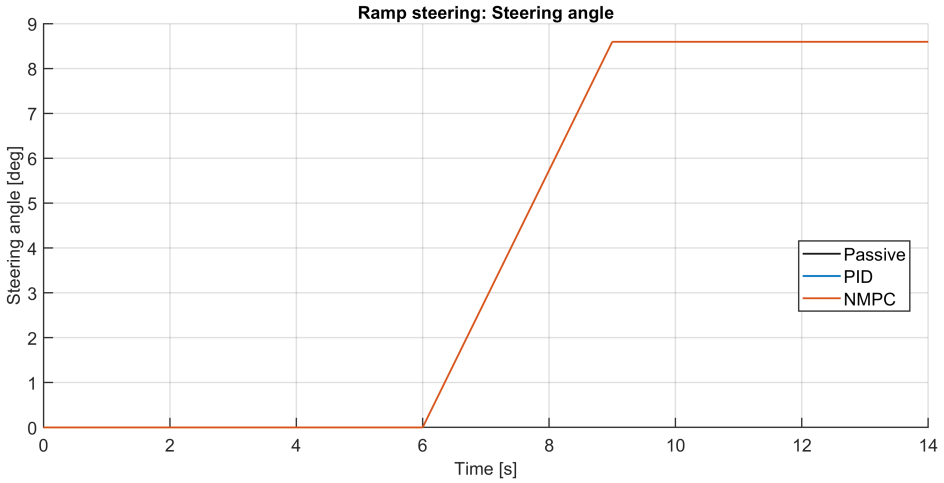

Figure 6.4: Ramp steering input

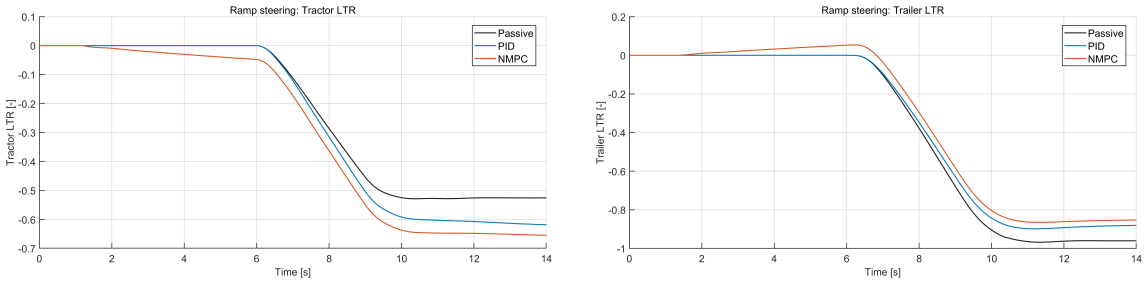

(a) Tractor LTR (b) Trailer LTR

Figure 6.5: LTR response under ramp steering

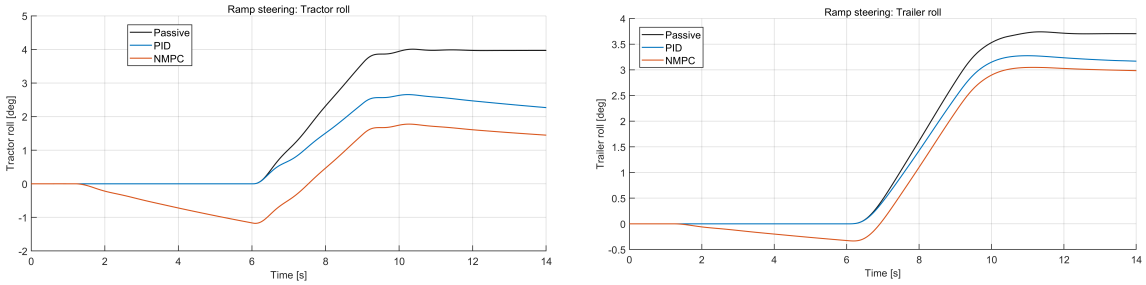

(a) Tractor roll (b) Trailer roll

Figure 6.6: Roll response under ramp steering

The ramp case yields a similar result with a smoother lateral buildup. The peak trailer LTR decreases from 0.968 with the passive suspension to 0.899 with PID and 0.865 with NMPC. The peak trailer roll angle decreases from 3.74° to 3.05°. The NMPC reductions are 10.6% in trailer LTR and 18.5% in trailer roll angle. No additional roll oscillation is visible in this test.

Case	tractor(Passive)	trailer(Passive)	tractor(NMPC)	trailer(NMPC)
Step steering	0.531	0.970	0.654	0.875
Ramp steering	0.529	0.968	0.655	0.865

Table 6.1: LTR trade-off summary

The same tractor–trailer trade-off appears in the ramp case. The tractor LTR increases from 0.529 to 0.655, while the trailer LTR decreases from 0.968 to 0.865. Table 6.1 therefore shows that the NMPC is not simply minimizing tractor roll. It is reallocating stability margin across the articulated combination. The tractor has more remaining margin, whereas the trailer is close to the critical load-transfer region. The controller uses this available tractor margin to pull the passive trailer farther away from the lift-off limit.

6.1.3 Directional Reversal: Lane Change

The lane-change case introduces a steering reversal, so the sign of the lateral load transfer changes during the maneuver. This is a difficult condition for a pneumatic suspension system because the actuator must not only generate force but also release and reverse it with precise timing.

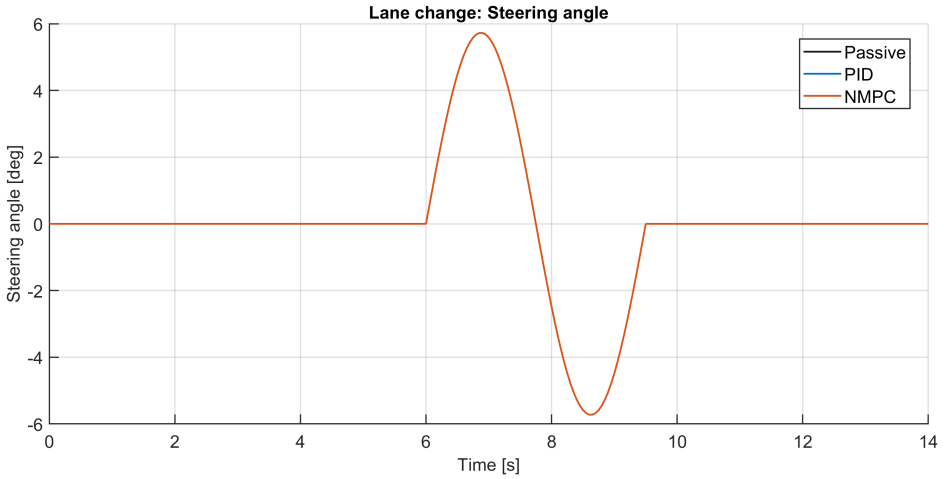

Figure 6.7: Lane-change input

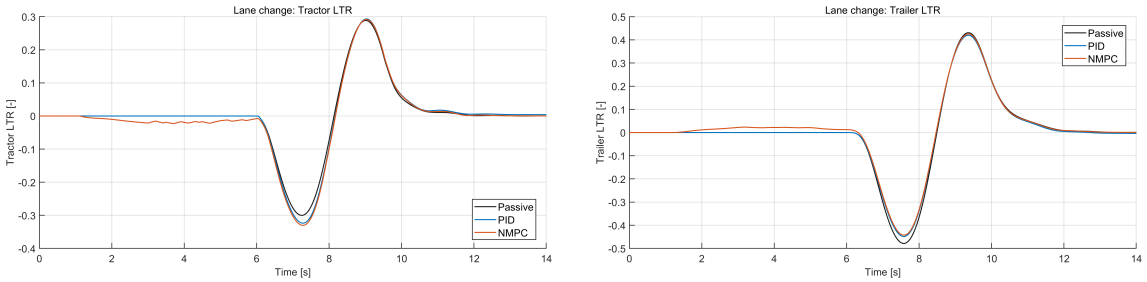

(a) Tractor LTR (b) Trailer LTR

Figure 6.8: Lane-change LTR comparison

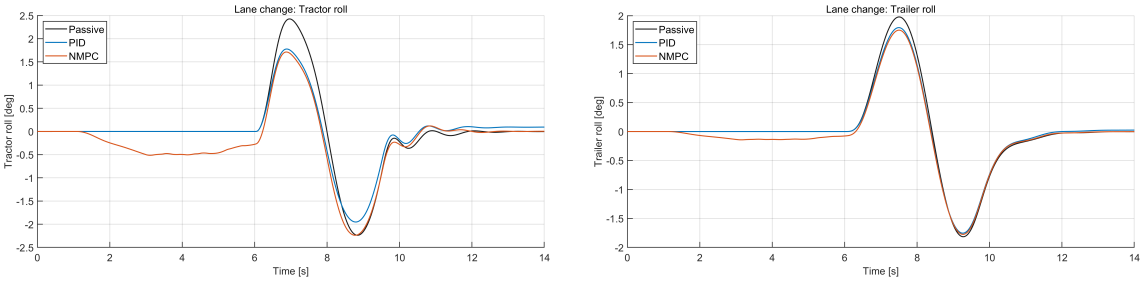

(a) Tractor roll (b) Trailer roll

Figure 6.9: Lane-change roll comparison

The lane-change peak values are lower than those in the step and ramp cases. The peak trailer LTR decreases from 0.479 with the passive suspension to 0.449 with PID and 0.443 with NMPC. The peak trailer roll angle decreases from 1.98° with the passive suspension to 1.78° with NMPC.

The key result is the behavior during load reversal. The NMPC uses the known steering input over its prediction window and begins changing the requested suspension force before the measured roll response has fully reversed. The reduction is smaller than in the step and ramp cases. The maneuver is farther from rollover, and the pneumatic force must change direction.

6.1.4 Slow Lane Change

A second lane-change test was added to examine a slower directional reversal. The vehicle speed is 10 m/s, and the peak steering angle is 0.10 rad. The steering action starts at $t = 4$ s and lasts 8 s.

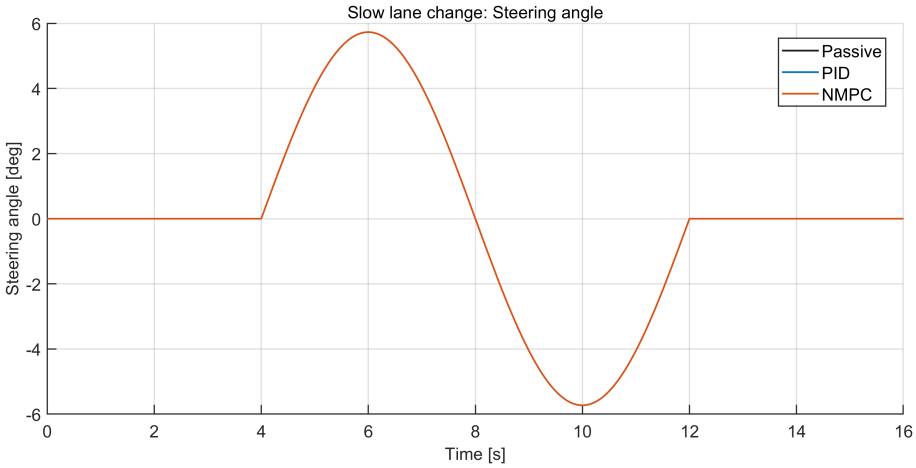

Figure 6.10: Slow lane-change input

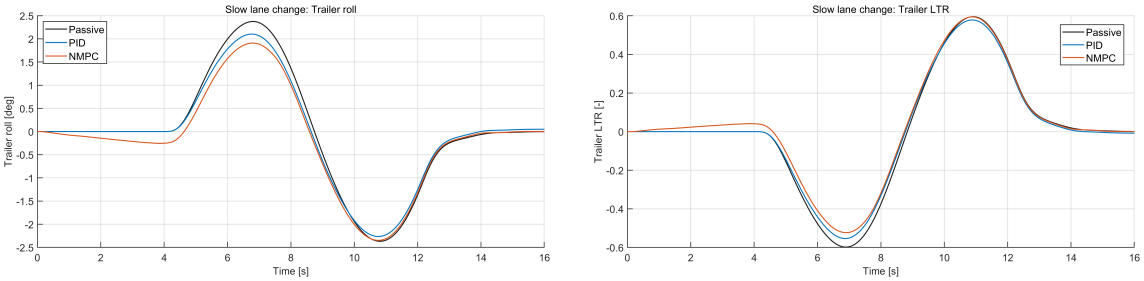

(a) Trailer roll (b) Trailer LTR

Figure 6.11: Slow lane-change responses

The passive, PID, and NMPC peak trailer roll angles are 2.375°, 2.264°, and 2.348°, respectively. Their maximum absolute trailer LTR values are 0.598, 0.579, and 0.595. Based solely on these overall peak values, NMPC reduces the maximum trailer roll by 1.1% and the maximum trailer LTR by 0.6% relative to the passive suspension, whereas PID yields the lowest overall peaks. However, the maximum absolute values do not fully capture the differences in controller behavior between the two steering phases.

During the first steering phase, NMPC clearly reduces the magnitude of the negative trailer LTR peak compared with both the passive suspension and PID. This confirms that the NMPC actively redistributes the tractor suspension forces and reduces the load transfer transmitted to the trailer. When the steering direction is reversed, however, the required redistribution of suspension forces must also reverse direction. Because the air-suspension actuators are subject to pressure dynamics, limited bandwidth, and force-rate constraints, the corrective force generated during the first steering phase cannot be reversed instantaneously. The remaining actuator response therefore delays the corrective action during the second turn.

Consequently, the positive trailer LTR peak during the second steering phase remains close to that of the passive suspension and is higher than the corresponding PID result. The slow lane-change case therefore does not indicate that NMPC is ineffective. Instead, it demonstrates that its performance depends on the relationship between the steering-reversal rate and the available actuator response speed. NMPC provides a clear benefit during the initial turn, but the rapid reversal of the required control action limits its effectiveness during the following turn.

6.1.5 Coupled Dynamics: Braking While Steering

The braking-while-steering case combines lateral and longitudinal load transfer. The steering input excites roll, while braking produces pitch and a forward load shift. This case therefore evaluates whether the controller can preserve trailer LTR margin when the vehicle is exposed to simultaneous roll and pitch dynamics.

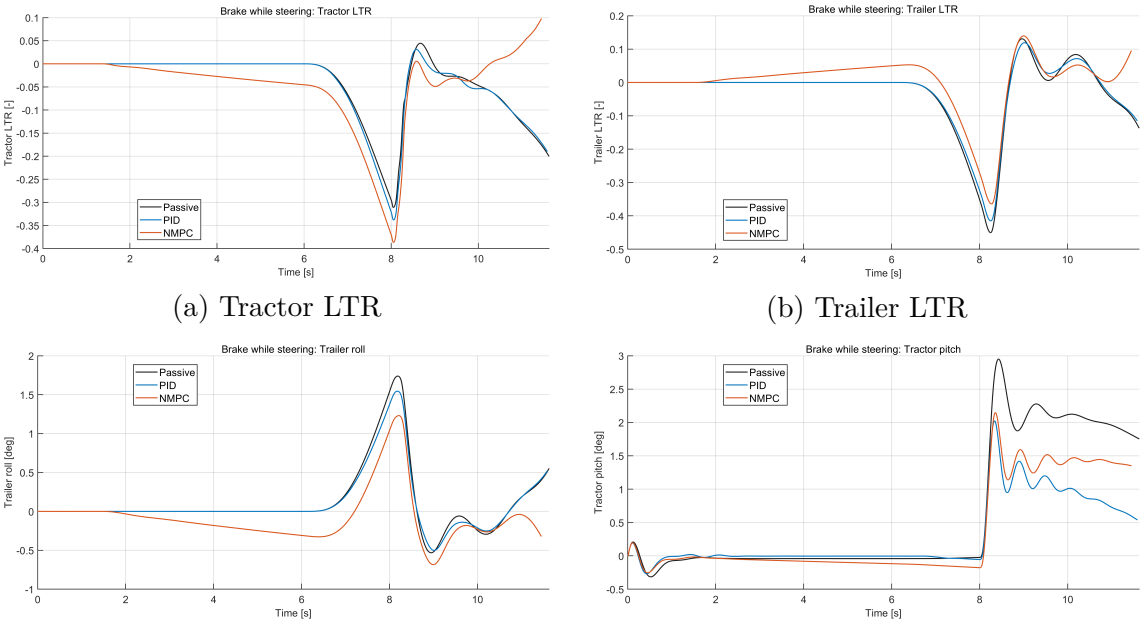

(a) Tractor LTR

(b) Trailer LTR

(c) Trailer roll

(d) Tractor pitch

Figure 6.12: Steering-braking response comparison

The coupled case gives the largest relative change in the current test set. The peak trailer LTR decreases from 0.451 for the passive baseline to 0.415 with PID and 0.364 with NMPC. The peak trailer roll angle decreases from 1.74° to 1.23°, corresponding to a 29.2% reduction. The tractor pitch peak also decreases from 2.95° with the passive suspension to 2.15° with NMPC.

This result shows the multi-objective character of NMPC. During braking, the controller must manage longitudinal load transfer while maintaining the lateral rollover margin. The NMPC does not simply minimize a single attitude angle; it selects suspension forces to keep the trailer LTR low even when the vertical load distribution is already being disturbed by the braking event.

6.2 Stability Boundary and LTR Surface

The time-domain results show the controller effect for selected maneuvers. The speed–steering sweep gives a broader view of the operating envelope by plotting trailer LTR as a function of vehicle speed and steering amplitude. This is useful because rollover safety is not determined by a single selected steering trace, but by the margin remaining before the vehicle reaches a critical load-transfer level.

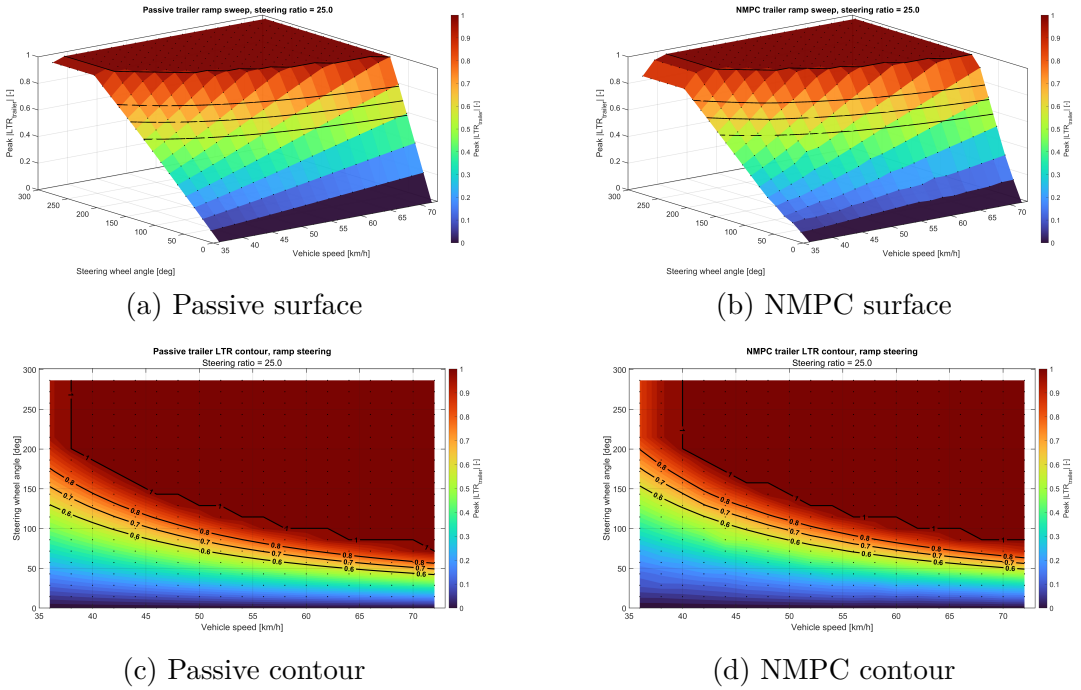

(a) Passive surface (b) NMPC surface

(c) Passive contour (d) NMPC contour

Figure 6.13: LTR surface comparison

The surfaces show that trailer LTR increases with both speed and steering amplitude. Compared with the passive case, the NMPC surface is lower in the high-LTR region. The tested sweep therefore indicates a shift in the high-risk part of the simulated operating envelope.

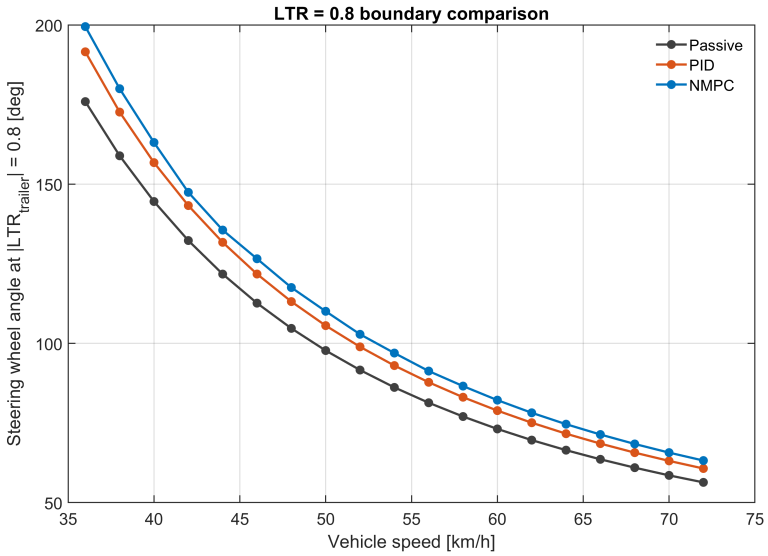

Figure 6.14: LTR boundary shift

At a steering wheel angle of approximately 80°, the passive baseline reaches the selected $|\mathrm{LTR}| = 0.8$ warning boundary at about 54 km/h. With NMPC, the same boundary is reached at approximately 60 km/h. The difference is about 6 km/h in

this sweep. More operating points are needed before this shift is treated as a general vehicle limit.

6.3 Handling Response and Trailer Rearward Behavior

After the rollover benefit has been established, the next question is whether the active suspension changes the intended handling behavior. This check is necessary because changing left–right vertical load distribution can influence tire cornering stiffness and therefore the apparent steering balance. The controller should improve rollover safety without creating a clear handling penalty.

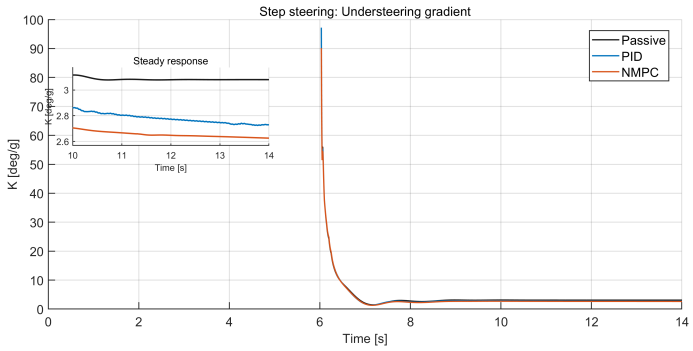

(a) Step

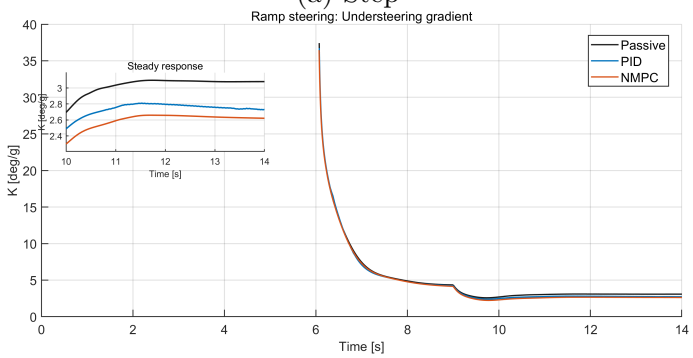

(b) Ramp

Figure 6.15: Understeer-gradient comparison

Figure 6.15 shows that the median understeer gradient decreases from about 3.08–3.09 deg/g with the passive suspension to about 2.65 deg/g with NMPC. This indicates a slightly less understeering response in these two tests. The steering-braking trace is harder to interpret because vehicle speed changes strongly. It is therefore used only as a supporting signal.

The following trailer lateral-acceleration plots and rearward-amplification table use the additional lateral-response metrics defined in Section 5.3.

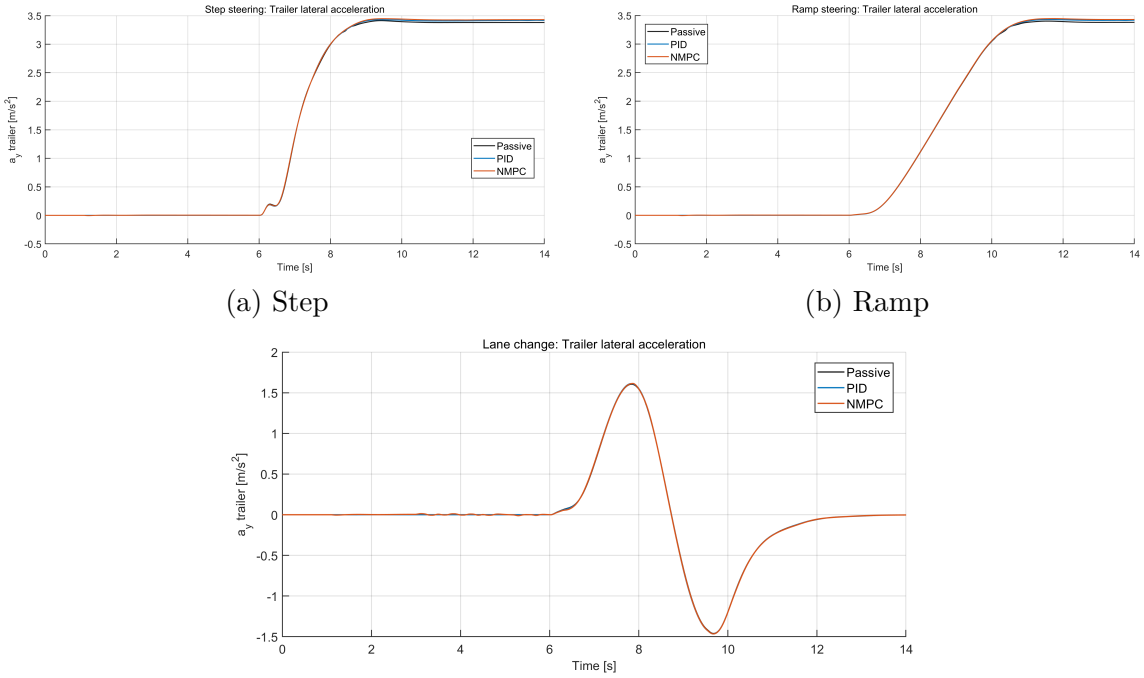

(a) Step

(b) Ramp

(c) Lane change

Figure 6.16: Trailer acceleration response

Case	Passive	PID	NMPC
Step steering	0.661	0.675	0.678
Ramp steering	0.959	0.961	0.961
Lane change	0.788	0.785	0.786
Braking while steering	0.425	0.592	0.476

Table 6.2: Rearward amplification summary

The trailer lateral acceleration changes only slightly between controllers. In step steering, the peak trailer lateral acceleration changes from 3.42 m/s^2 to 3.45 m/s^2; in ramp steering, it changes from 3.40 m/s^2 to 3.45 m/s^2. These changes are much smaller than the roll and LTR reductions. The rearward amplification values in Table 6.2 also remain close for the steering-only cases. This supports the interpretation that NMPC mainly redistributes vertical load and rollover margin, rather than simply weakening the lateral maneuver or exciting the trailer more strongly.

6.4 Trajectory and Braking Distance

The logged x and y coordinates are used to compare the response to the same open-loop steering input. There is no target path and no path-tracking controller in these tests.

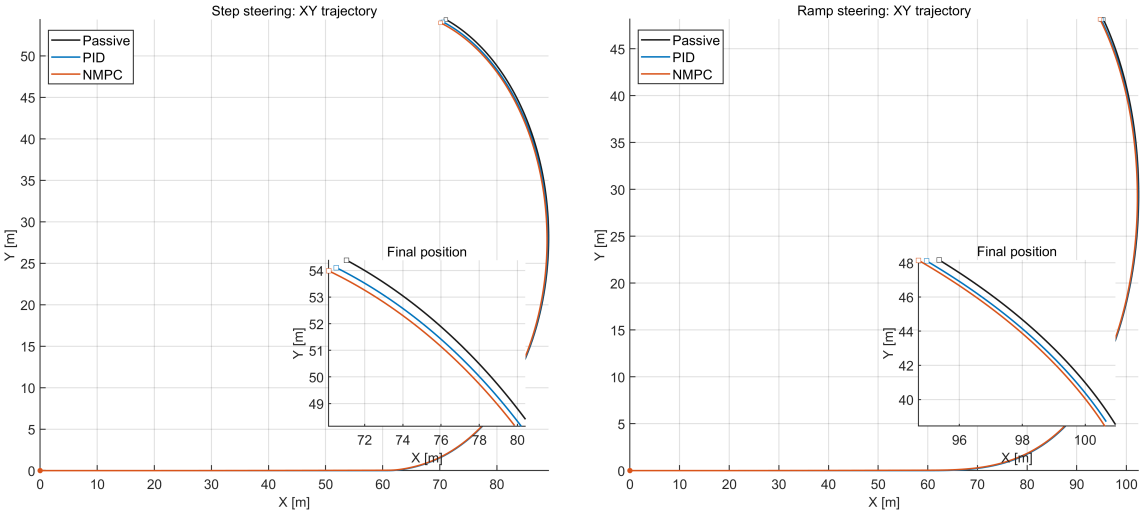

(a) Step (b) Ramp

Figure 6.17: Step and ramp trajectories

Figure 6.17 shows the step and ramp trajectories. The endpoint insets make the small final-position differences visible. These plots show only how suspension control affects the open-loop vehicle response.

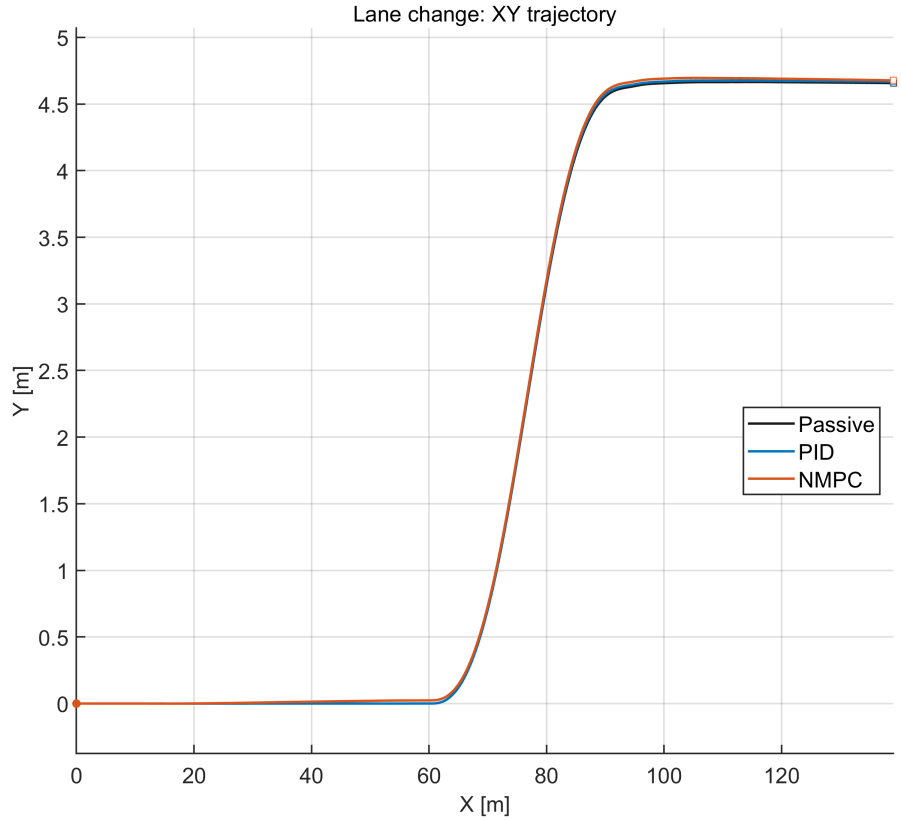

Figure 6.18: Lane-change trajectory

Figure 6.18 shows the path during the steering reversal. The vertical axis is limited to the range reached by the three simulated trajectories, with a small margin around

the data.

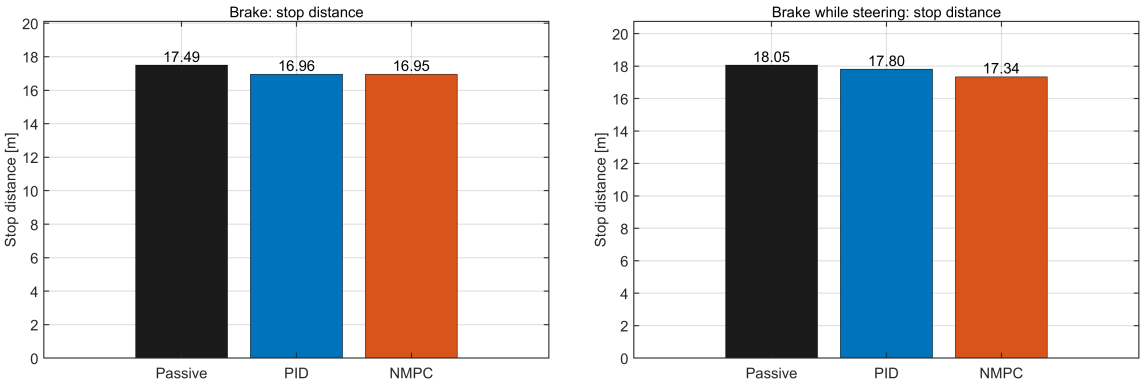

(a) Straight braking (b) Steering-braking

Figure 6.19: Stopping distance comparison

The earlier distance calculation included travel before the brake command. Figure 6.19 uses the corrected interval from brake-command onset until $v_x \leq 0.05$ m/s. In straight braking, the passive, PID, and NMPC distances are 17.49 m, 16.96 m, and 16.95 m. In steering-braking, the corresponding values are 18.05 m, 17.80 m, and 17.34 m. These values are calculated from the cumulative x-y path within the braking interval.

6.5 Overall Discussion

Case	Trailer roll	Trailer LTR	Main interpretation
Step steering	−16.9%	−9.8%	Severe transient control
Ramp steering	−18.5%	−10.6%	Smooth build-up control
Lane change	−10.3%	−7.5%	Roll reversal control
Slow lane change	−1.1%	−0.6%	PID gives lower peaks
Braking while steering	−29.2%	−19.2%	Coupled load transfer

Table 6.3: NMPC result summary

Table 6.3 summarizes the percentage changes in peak trailer roll and trailer LTR achieved by the NMPC relative to the passive suspension. The controller provides the greatest improvement during combined steering and braking, where both lateral and longitudinal load transfer are present. In contrast, the improvement is limited in the slow lane-change case, indicating that the benefit of predictive control depends on the maneuver's time scale and severity.

NMPC gives the lowest peak trailer roll and trailer LTR in the step, ramp, standard lane-change, and steering-braking cases. The largest changes occur near the selected LTR warning region and during combined steering and braking.

The revised controller includes pneumatic force-rate limits and tractor–semitrailer coupling in the same optimization. It can use some of the tractor load-transfer margin while reducing the more critical trailer LTR. This explains why tractor LTR can increase while trailer LTR decreases.

The understeer gradient changes slightly, while trailer lateral acceleration, rearward amplification, and the open-loop trajectory remain close to the passive case. The braking distance is calculated from the onset of brake command to the stopping threshold. The completed slow lane change also shows that controller ranking depends on the time scale of the steering input.

7

Conclusions and Future Work

7.1 Conclusion

The main result of this thesis is that the revised NMPC can improve the simulated rollover margin of the passive semitrailer using active suspension forces generated only on the tractor. In the severe steering-only cases, the peak trailer LTR is reduced from 0.970 to 0.875 in step steering and from 0.968 to 0.865 in ramp steering. The corresponding peak trailer roll reductions are 16.9% and 18.5% relative to the passive baseline. In the standard lane change, the peak trailer LTR decreases from 0.479 to 0.443, while the peak trailer roll angle decreases from 1.98° to 1.78°.

The clearest benefit is obtained when steering and braking are combined. In this case, NMPC reduces the peak trailer LTR from 0.451 to 0.364 and the peak trailer roll angle from 1.74° to 1.23°. The tractor pitch peak also decreases from 2.95° to 2.15°. In the speed–steering sweep, the selected $|\mathrm{LTR}| = 0.8$ warning boundary at approximately 80° steering-wheel angle shifts from about 54 km/h with passive suspension to about 60 km/h with NMPC.

The improvement is achieved by reallocating load-transfer margin within the articulated combination rather than by reducing all tractor responses. In the step and ramp cases, the tractor LTR increases while the trailer LTR decreases, indicating that the controller uses the available tractor-side margin to reduce the more critical semitrailer response. The handling checks show only small changes in trailer lateral acceleration, rearward amplification, and open-loop trajectory, so the LTR reductions are not mainly caused by a weakened lateral maneuver.

7.2 Future Work

While the developed predictive control framework exhibits substantial promise in simulation, several key areas remain for future research to facilitate practical implementation and expand system capabilities:

1. Practical vehicle deployment will necessitate the integration of a comprehensive state estimation and preview generation layer. Because the current controller assumes idealized access to full state feedback and to future driver actions from the simulation environment, developing robust state observers is crucial for reconstructing unmeasurable quantities in the presence of realistic

sensor noise and bias.

2. The operational robustness of the active suspension system should be extensively verified under a wider envelope of external disturbances and parametric uncertainties. Assessing the controller's adaptation to large payload variations, shifting centers of gravity, and fluctuating tire–road friction coefficients will clarify the performance boundaries. This investigation would establish whether supplementary robust control techniques or adaptive internal models are required to maintain stability margins in unpredictable environments.

3. The evaluation framework should be expanded to incorporate three-dimensional road topographies and full vertical vehicle dynamics. Future iterations should evaluate the suspension performance on realistic uneven surfaces, rough terrain, and sloped highway transitions to thoroughly investigate the classical trade-off between active rollover prevention and high-frequency vibration isolation, thereby ensuring that ride comfort is not unduly compromised by roll-stabilizing force inputs.

4. Extending the predictive framework to coordinate the active air suspension with torque vectoring and active differentials within a unified chassis dynamics layer represents a highly promising direction. Investigating how the continuous distribution of driving forces and active differential locking torque can be optimized alongside the vertical suspension forces would provide a more integrated approach to motion control, effectively managing the intense yaw–roll coupling during extreme maneuvers and further maximizing the vehicle's safe handling boundaries.

5. The previous and revised NMPC formulations should be compared under the same tractor–semitrailer configuration, payload, actuator constraints, and driving maneuvers. Such a comparison would clarify how the added pitch dynamics, hitch coupling, four-corner force control, and pressure-dependent force-rate constraints affect vehicle stability, actuator effort, and computational performance.

Bibliography

[1] B. Jacobson et al., *Vehicle Motion Engineering*, Chalmers University of Technology, draft compendium, 2024.

[2] NZ Transport Agency Waka Kotahi, *Heavy Vehicle Stability Guide*, Version 1.0, accessed 2026.

[3] C. B. Winkler, D. Blower, R. D. Ervin, and R. M. Chalasani, *Rollover of Heavy Commercial Vehicles*, SAE Research Report RR-004, UMTRI-99-19, 2000.

[4] Ta Tuan Hung, *A Simulation Approach to Determine Dynamic Rollover Threshold of a Tractor Semi-Trailer Vehicle during Turning Maneuvers*, Master's thesis, Chalmers University of Technology, 2024.

[5] Y. Hou and M. Ahmadian, "Effects of Commercial Truck Configuration on Roll Stability in Roundabouts," *SAE Technical Paper 2015-01-2741*, 2015. doi: 10.4271/2015-01-2741.

[6] V. T. Vu, O. Sename, L. Dugard, and P. Gaspar, "Enhancing roll stability of heavy vehicle by LQR active anti-roll bar control using electronic servo-valve hydraulic actuators," *Vehicle System Dynamics*, vol. 55, no. 9, pp. 1405–1429, 2017. doi: 10.1080/00423114.2017.1317822.

[7] S. Kharrazi, *Steering Based Lateral Performance Control of Long Heavy Vehicle Combinations*, PhD dissertation, Chalmers University of Technology, Gothenburg, Sweden, 2012. ISBN: 978-91-7385-724-6.

[8] Y. Chen and M. Ahmadian, "Countering the destabilizing effects of shifted loads through pneumatic suspension design," *SAE International Journal of Vehicle Dynamics, Stability, and NVH*, vol. 4, no. 1, pp. 5–17, 2020. doi: 10.4271/10-04-01-0001.

[9] D. J. M. Sampson and D. Cebon, "Achievable roll stability of heavy road vehicles," *Proceedings of the Institution of Mechanical Engineers, Part D: Journal of Automobile Engineering*, vol. 217, no. 4, pp. 269–287, 2003. doi: 10.1243/09544070360613237.

[10] S. Lee and J. Olsson, *Active Air Suspension Modeling and Control for Roll Stability in Heavy-duty Vehicles*, Master's thesis, Chalmers University of Technology, 2025.

[11] T. T. Hung and D. N. Khanh, "Multibody system dynamics analysis method approach to determine dynamic roll early warning and control thresholds of tractor semi-trailer vehicles," *Journal of Vibration Engineering & Technologies*, vol. 13, no. 2, 2025. doi: 10.1007/s42417-024-01592-w.

[12] P. Anistratov, *Autonomous Avoidance Maneuvers for Vehicles using Optimization*, PhD dissertation, Linkoping University Electronic Press, Linkoping, 2021. doi: 10.3384/diss.diva-176515.

[13] M. N. Azadani and A. Boukerche, "A novel multimodal vehicle path prediction method based on temporal convolutional networks," *IEEE Transactions on Intelligent Transportation Systems*, vol. 23, no. 12, pp. 25384–25395, 2022. doi: 10.1109/TITS.2022.3151263.

[14] C.-P. Larten, *Modeling and Identification of Air Suspension in Heavy-Duty Vehicles*, Master's thesis, Linkoping University, Department of Electrical Engineering, 2016.

[15] A. A. Shabana, *Dynamics of Multibody Systems*, 5th ed. Cambridge: Cambridge University Press, 2020.

[16] A. J. Nieto, A. L. Morales, A. Gonzalez, J. M. Chicharro, and P. Pintado, "An analytical model of pneumatic suspensions based on an experimental characterization," *Journal of Sound and Vibration*, vol. 313, no. 1–2, pp. 290–307, 2008. doi: 10.1016/j.jsv.2007.11.027.

[17] Y. Chen, M. Ahmadian, and A. Peterson, "Pneumatically balanced heavy truck air suspensions for improved roll stability," *SAE Technical Paper 2015-01-2749*, 2015. doi: 10.4271/2015-01-2749.

[18] X. Sun, Y. Cai, S. Wang, Y. Liu, and L. Chen, "A hybrid approach to modeling and control of vehicle height for electronically controlled air suspension," *Chinese Journal of Mechanical Engineering*, vol. 29, no. 1, pp. 152–162, 2016. doi: 10.3901/CJME.2015.1202.141.

[19] Volvo Group Trucks Technology, *Volvo Truck Model, Simulink Library*, Developed at Volvo Group Trucks Technology, 2023.

[20] Volvo Trucks, *VTM Plant Model Description*, unpublished internal company document, 2018.

[21] M. K. Aripin, Y. Md Sam, K. A. Danapalasingam, K. Peng, N. Hamzah, and M. F. Ismail, "A review of active yaw control system for vehicle handling and stability enhancement," *International Journal of Vehicular Technology*, 2014. doi: 10.1155/2014/437515.

[22] W. Cho, J. Suh, and S.-H. You, "Integrated motion control using a semi-active damper system to improve yaw-roll-pitch motion of a vehicle," *IEEE Access*, vol. 9, pp. 52464–52473, 2021. doi: 10.1109/ACCESS.2021.3070366.

[23] M. Ricco, A. Alshawi, P. Gruber, M. Dhaens, and A. Sorniotti, "Nonlinear model predictive control for yaw rate and body motion control through semi-active and active suspensions," *Vehicle System Dynamics*, vol. 62, no. 6, pp. 1587–1620, 2024. doi: 10.1080/00423114.2023.2251615.

[24] Y. Chen, A. W. Peterson, and M. Ahmadian, "Achieving anti-roll bar effect through air management in commercial vehicle pneumatic suspensions," *Vehicle System Dynamics*, vol. 57, no. 12, pp. 1775–1794, 2019. doi: 10.1080/00423114.2018.1552005.

[25] D. J. M. Sampson, "Active roll control of articulated heavy vehicles," PhD dissertation, Department of Engineering, University of Cambridge, 2000.

[26] A. J. P. Miege and D. Cebon, "Optimal roll control of an articulated vehicle: theory and model validation," *Vehicle System Dynamics*, vol. 43, no. 12, pp. 867–884, 2005. doi: 10.1080/00423110500217167.

[27] P. Gaspar, I. Szaszi, and J. Bokor, "Improving rollover stability with active suspensions by using an LPV method," *IFAC Proceedings Volumes*, vol. 37, no. 8, pp. 781–786, 2004. doi: 10.1016/S1474-6670(17)32075-X.

[28] X. Sun, C. Yuan, Y. Cai, S. Wang, and L. Chen, "Model predictive control of an air suspension system with damping multi-mode switching damper based on hybrid model," *Mechanical Systems and Signal Processing*, vol. 94, pp. 94–110, 2017. doi: 10.1016/j.ymssp.2017.02.033.

[29] Y. Jeong, "Integrated vehicle controller for path tracking with rollover prevention of autonomous articulated electric vehicle based on model predictive control," *Actuators*, vol. 12, no. 1, article 41, 2023. doi: 10.3390/act12010041.

[30] Y. Zhou, Z. Li, W. Yu, and Y. Yu, "Cooperative control of interconnected air suspension based on model predictive control," *Applied Sciences*, vol. 12, no. 19, article 9886, 2022. doi: 10.3390/app12199886.

[31] S. Yim, "Design of a preview controller for vehicle rollover prevention," *IEEE Transactions on Vehicular Technology*, vol. 60, no. 9, pp. 4217–4226, 2011. doi: 10.1109/TVT.2011.2169687.

DEPARTMENT OF ELECTRICAL ENGINEERING
CHALMERS UNIVERSITY OF TECHNOLOGY
Gothenburg, Sweden
www.chalmers.se

CHALMERS
UNIVERSITY OF TECHNOLOGY